Journal of Molecular Liquids 369 (2023) 120921

Contents lists available at ScienceDirect

Journal of Molecular Liquids

journal homepage: www.elsevier.com/locate/molliq

Synthesis, molecular docking and anticancer potential of azolium based salts and their silver complexes: DNA/BSA interaction studies and cell cycle analysis

Rizwan Ashraf [a,*], Ayesha Sarfraz [a], Tugba Taskin-Tok [b,j], Muhammad Javid Iqbal [c], Muhammad Adnan Iqbal [a], Jamshed Iqbal [d], Haq Nawaz Bhatti [a,*], Mohamed El-Naggar [e,f], Sumia Akram [g], Mohammad N. Murshed [h], Mohamed E. El Sayed [h], Ahmed Samir [h,i]

[a] Department of Chemistry, University of Agriculture Faisalabad, Faisalabad 38000, Pakistan
[b] Gaziantep University, Faculty of Arts and Sciences, Department of Chemistry, +9027310 Gaziantep, Turkey
[c] Department of Chemistry, COMSATS University Islamabad, Lahore Campus, Defense road, Lahore, Pakistan
[d] Center for Advanced Drug Research, COMSATS University Islamabad, Abbottabad Campus, Abbottabad 22060, Pakistan
[e] Chemistry department, Faculty of Sciences, Pure and Applied Chemistry Group, University of Sharjah, P. O.Box 27272, Sharjah, United Arab Emirates
[f] National Institute of Oceanography and Fisheries, kayet Bay, Alexandria, Egypt
[g] Division of Science and Technology, University of Education Lahore, Lahore, Pakistan
[h] Physics Department, Faculty of Science and Arts, King Khalid University, Muhayl Asser, Saudi Arabia
[i] Center of Plasma Technology, Al-Azhar University, Cario, Egypt
[j] Gaziantep University, Institute of Health Sciences, Department of Bioinformatics and Computational Biology, 9027310, Gaziantep Turkey

ARTICLE INFO

Article history:
Received 22 August 2022
Revised 16 November 2022
Accepted 25 November 2022
Available online 28 November 2022

Keywords:
Molten salts
Ag(I)-complex
Molecular docking study
MTT assay
ROS generation assay
DNA interaction study

ABSTRACT

Azolium based molten salts have widely been investigated for biological potentials and interestingly, their metal complexes are getting attention in the field of medicinal inorganic chemistry. Here, we report three binuclear molten salts (**L1-L3**) and their silver complexes (**C1-C3**), assured through spectroscopic and mass spectrometric approaches. Solvent dependent catecholase activity was studied in three different solvents which suggests that nature of solvent has potential impact on chemical reactivity of test compounds. Anticancer activity was investigated through MTT assay, fluorescence microscopic analysis, ROS generation, and cell cycle arrest assay against HeLa, MCF-7, HCT-116 and A549 cancer cell lines and results confirmed the superior anticancer potential of silver complexes from their precursor salts. The cytotoxicity was cell selective and dose-dependant against MCF-7 with IC_{50} of C1 6.28 ± 0.82 μM which outshone even from positive control 5-FU (12.87 ± 1.0 μM) and cisplatin (8.74 ± 0.52 μM). Biological behavior of C1 & C2 was predicted through molecular docking studies and it speculated lower binding energies of C1 *i.e.* −10.05 kcal/mol and −7.51 kcal/mol for DNA and BSA, respectively. The experimental study of drug-DNA and drug-BSA interaction confirmed the prediction of simulation results. In addition, the role of hydrophobicity of compounds in the cytotoxicity was established viz., how the lipophilic value affects the anticancer activity of complexes.

1. Introduction

Benz-imidazole based derivatives is a class of *N*-heterocyclic compounds that have the ability for synthesis of highly efficient ionic liquids and molten salts. Benz-imidazolium salts have been widely reported for their beneficial use of biological agents, medicines, especially antibiotic, anti-inflammatory and antioxidants etc. but scarcely found as good anticancer agents [1]. Metal complexes have shown astonishing bioactive functions as an anticancer agents but the choice of ligand is a key deicidal for the bioactivity of metallo drugs [2,3]. Furthermore, ligand design affects safety profile, permeability via cell membrane through lipophilic character, stability, release of metal center and related side effects [4]. Interestingly, Benz-imidazolium compounds have carbene carbon and acidic proton making them strong candidates

Abbreviations: ROS, Reactive oxygen species; DNA, Deoxyribonucleic acid.

* Corresponding authors.
E-mail addresses: rizi_chem82@hotmail.com (R. Ashraf), haq_nawaz@uaf.edu.pk (H.N. Bhatti).

https://doi.org/10.1016/j.molliq.2022.120921
0167-7322/

for synthesis of metal complexes for desired properties [1,5]. Moreover, the chain length of these compounds affects the lipophilic character and biological reactivity, toxicity, selectivity and intensity of interaction with biomolecules which are important traits of medicinal compounds [6,7]. Therefore, azolium based molten salts or ionic liquids could be judicious choice for the synthesis of metal complexes in the quest of effective anticancer agents. Our group has previously reported *N*-heterocyclic carbene complexes (NHCs) with Silver, Nickle, Gold as well as Selenium adducts [6,8–11].

It is believed that proteins and DNA are the primary cellular target for cytotoxicity of metal based anticancer agents as their interaction could block or damage DNA leads to apoptosis [12]. For drug proteins interaction, in biological fluids, serum albumin is most extensively studying protein as it is abundant model protein in plasma (contributes 52% of total composition of circulatory system proteins) play an important role of transportation of endogenous species [13]. Our previous studies and literature reports have confirmed that silver-NHC complexes have high binding ability with proteins and DNA and therefore, assessment of this binding ability could be important prior tool to investigate anticancer potentials [11]. In addition to biomolecular interaction, lipophilicity or electron density on aromatic ring system may effect in cytotoxicity [14]. In this context, we have sought to correlate structural behavior of studied complexes in lipophilicity, stability in solution form and protein/DNA interactions related to cytotoxicity.

With above discussions and expansion of our ongoing research, we designed benzimidazolium derivatives with aliphatic side chain (**L1-L3**) and their silver complexes (**C1-C3**) to investigate their cytotoxic potential against MCF-7, HeLa, A549 and HCT-116 cell lines through fluorescent microscopic aided MTT assay and ROS generation assay. Flow cytometry was used to measure cell cycle arrest assay against HeLa and MCF-7 cell lines. The studied compounds were also computed through molecular docking calculations and confirmed through spectroscopic and viscosity based studied for interaction with BSA/DNA molecules.

2. Materials and methods

All the chemicals used for present study including benzimidazole, paraxylenedibromide, 1-bromo-2-methylbutane, 1-bromo octane, 1-bromo decane and potassium hydroxide were of synthesis grade procured from Sigma Aldrich (Germany), via indigenous supplier Analytics-Pakistan. Silver powder (Ag_2O) of synthesis grade was procured from avonchem (United Kingdom). Solvents including Methanol, Dimethyl sulfoxide (DMSO), diethyl ether, 1,4-dioxane, petroleum ether and chloroform were of solvent grade procured from Merck-milipore Germany used as such as received. All the synthesized compounds were characterized through ATR-FTIR (IRTracer-100, Shimadzu Japan), UV–Visible spectrophotometer (UV 1800/UV–vis, Shimadzu Japan). ^{1}H &^{13}C NMR spectroscopy (Burker, Avance NMR spectrometer).

*2.1. 1,4-bis((benzimidazol-1-yl)methyl)benzene (P-**I**)*

Initially, Benz-imidazole (6 g, 0.051 mol) and KOH (3 g, 0.054 mol) were mixed in 30 mL of solvent (DMSO) and further stirred for 30 min at ambient conditions. Reaction mixture was being added with 1,4-dibromo-p-xylene (3 g, 0.011 mol) stirred for 5 h at room temperature [9]. Yield: 94%. M.P: 132.8 °C. UV–vis. (λ^{max}, nm): 260.0, 275.0. ^{1}H NMR (400.0 MHz, $DMSO_{d6}$, δppm), 5.45(s, 4H, NCH_2), 7.17(m, 4H, Ar-H), 8.36 (s, 2H, NCHN). ^{13}C NMR (110 MHz, $DMSO_{d6}$, δppm), 48.0 (2C, NCH_2), 110.6, 120.0, 122.1, 128.0, 130.2 (16C, Ar-C), 146.8 (2C, NCN). ESI-MS (*m*/*z*): $[M + 1]^+$ Calc. for $[C_{22}H_{19}N_4]$ = 339.15 Da, Found = 339.33 Da. Ana. Cal. for $[C_{22}H_{18}N_4]$: C 78.08; H 5.36; N 16.56. Found: C 77.98; H 5.34; N 16.58.

*2.2. 1,4-bis((3-(2-methylbutyl)-2,3-dihydrobenzimidazol-1-yl) methyl)benzene bromide salt (**L1**)*

Precursor-I (1 g, 2.95 mmol) and 1-bromo-2-methylbutane (0.88 g, 5.91 mmol) were refluxed in 1,4-dioxane for 24 h reaction [15], greyish product settled down. Yield: 91.2%. UV–vis. (λ^{max}, nm), 278.00 (π-π*), 288.00 (n-π*). FLR emission (λ^{max}, nm) 362.0 (excitation 254 nm). FTIR (ATR cm^{-1}): 2955 (C_{arom}-H strch), 2920 (C_{aliph}-H strch), 1489, 1432 (C—C strch), 1260 (C—N strch), 734 (C—H bend). ^{1}H NMR (400 MHz, $DMSO_{d6}$, δppm), 0.96(d, 12H, C_{Aliph}-H_3), 1.84(m, 4H, C_{aliph}-H), 4.50(q, 4H, N-CH_2), 7.54(s, 4H, Ar-H), 9.95(s, 2H, HCN_2). ^{13}C NMR (110 MHz, $DMSO_{d6}$, δppm), 22.9(4C, CH_3), 49.0(2C, N-CH_2), 110.0, 120.0, 127.0, 130.0 (20C, Ar-C), 143.0 (4C, N-CH_2) 144.0 (2C, NCN). ESI-MS (*m*/*z*): $[M-2Br-H]^+$ Calculated for $[C_{32}H_{41}N_4]^+$ = 481.32 Da, Found = 481 .33 Da. Ana. Cal. for $[C_{32}H_{42}Br_2N_4]$: C 59.89; H 06.59; Br 24.87; N 08.72. Found: C 59. 86; H 06.52; N 08.81.

*2.3. 1,4-bis((3-octyl-2,3-dihydrobenzimidazol-1-yl)methyl)benzene, bromide salt (**L2**)*

Precursor-I (1.5 g, 4.43 mmol) and 1-bromooctane (2.3 g, 11.89 mmol) was reacted under same conditions for 24 h as for **L1.** Yield: 89.8%. UV–vis (λ^{max}, nm): 285.00 and 299.00. FLR emission (λ^{max}, nm): 350.0. FTIR (ATR cm^{-1}): 2931, 2860 (C—H strch), 1558 (C=C strch), 1449 (C—C strch), 1230, 1153 (C—N strch), 715, 655 (C—H bend). ^{1}H NMR (400 MHz, $DMSO_{d6}$, δppm), 1.43(t, 4H, C_{aliph}-H_2), 4.01(d, 4H, N-CH_2), 8.50(m, 4H, Ar-H), 10.57(s, 2H, HCN_2). ^{13}C NMR (110 MHz, $DMSO_{d6}$, δppm), 14.1(2C, CH_3), 50.0 (2C, N-CH_2), 110.0(16C, Ar-C), 141.3(2C, NCN). ESI-MS (*m*/*z*): $[M-2Br + H]^+$ Cal. for $[C_{38}H_{55}N_4]^+$ = 567.43 Da, Found 567.33 Da. Ana. Cal. for $[C_{38}H_{54}Br_2N_4]$: C 62.81; H 7.49; Br 21.99; N 7.71. Found: C 62.80; H 7.40; N 7.70.

*2.4. 1,4-bis((3-decyl-2,3-dihydrobenzimidazol-1-yl)methyl)benzene, bromide salt (**L3**)*

Precursor-I (1 g, 2.95 mmol) and 1-bromodecane (1.30 g, 5.91 mmol) was reacted under same conditions for 22 h as followed for **L1**. Yield: 88.3%. UV–vis (λ^{max}, nm): 265.00, 288.00 (π-π*and n-π*) respectively. FLR emission (λ^{max}, nm) 353.0. FTIR (ATR cm^{-1}): 2921, 2852 (C—H strch), 1559 (C=C strch), 1423 (C—C strch), 1220, 1198 (C—N strch), 780, 722 (C—H bend). ^{1}H NMR (400 MHz, $DMSO_{d6}$, δppm), 0.84(t, 6H, CH_3), 1.27(m, 20H, $C_{Aliph}H_2$), 1.91(m, 4H, $C_{aliph}H_2$), 8.10(d, 4H, Ar-H), 10.02(s, 2H, HCN_2). ^{13}C NMR (110 MHz, $DMSO_{d6}$, δppm), 15.0(2C, CH3), 52.0 (2C, N-CH_2), 113.4, 126.0, 135.0, 138.0(14C, Ar-C), 151.0(2C, NCN). ESI-MS (*m*/*z*): $[M-2Br + H]^+$ Cal. for $[C_{42}H_{65}N_4]^+$ = 609.98 Da, Found 610.08 Da. Ana. Cal. for $[C_{42}H_{64}Br_2N_4]$: C 64.44; H 7.98; Br, 20.42; N 7.16. Found: C 64.40; H 7.91; N 7.13.

*2.5. 1,4-bis((3-(2-methylbutyl)-2,3-dihydrobenzimidazol-1-yl) methyl)benzene, silver hexafluoro phosphate (**C1**)*

L1 (0.5 g, 0.78 mmol) and Ag_2O (0.36 g, 1.56 mmol) were dissolved in 100 mL of methanol was stirred in the absence of light at room temperature for 48 h. The product was filtered through filter paper and Celite column, halide counter ions were directly replaced by $PF6^-$ ions upon reaction with aqueous potassium hexaflouro phosphate (0.24 g, 1.32 mmol) at room temperature for 2 h with continuous stirring. Immediately, precipitation occurred. Precipitates were washed and dried. Yield: 83%. M.P 183.4 °C. UV–vis (λ^{max}, nm): 283.00, 288.00 (π-π*and n-π*). FLR emission (λ^{max}, nm)

278.0. FTIR (ATR cm^{-1}): 2956 (C—H strch), 1617, 1567 (C═C strch), 1479 (C-Ag strch), 1399 (C—C strch) 1193 (C—N strch), 741(C—H bend). ^{1}H NMR (400 MHz, $DMSO_{d6}$, δppm), 0.91(d, 24H, $C_{aliph}H_3$), 1.75(m, 8H, $C_{Aliph}H_2$), 4.57 (m, 4C, NCN), 5.7 (s, 8H, N-CH_2), 8.02 (m, 8H, Ar-H).^{13}C NMR (110 MHz, $DMSO_{d6}$, δppm), 22.9 (8C, CH_3), 49.0 (4C, N-CH_2), 111.4, 123.9, 128.0, 137.6(24C, Ar-C), 178.8 (4C, N_2C-Ag). ESI-MS (m/z):$[M + 1]^+$ Cal. for $[C_{64}H_{81}Ag_2N_8]^+$ = 1162.21 Da, Found: 1162.50 Da. HPLC purity: 99.49%. Ana. Cal. for $[C_{64}H_{80}Ag_2N_8]^+$:C 52.40; H 5.50; Ag 14.71; F 15.54; N 7.64; P 4.22. Found: C 52.42; H 5.45; N 7.60.

2.6. 1,4-bis((3-octyl-2,3-dihydrobenzimidazol-1-yl)methyl)benzene, silver hexafluorophosphate (*C2*)

L2 (0.7 g, 0.96 mmol) and Ag_2O (0.44 g, 1.89 mmol) were dissolved in 100 mL of methanol was reacted by following the same procedure as used for **C1.** Light gray powder was obtained. Yield: 88%. M.P 192.8 °C. UV–vis (λ^{max}, nm): 250.00 (π-π*). FLR emission (λ^{max}, nm) 340.0. 298 nm. FTIR (ATR cm^{-1}): 2900 (C—H strch), 1560 (C═C strch), 1456 (C-Ag strch) 1238, 1153 (C—N strch), 825, 655 (C— H bend). ^{1}H NMR (400 MHz $DMSO_{d6}$, δppm), 0.64(t, 12H, C_{Alip}-H_3), 1.23(m, 32H, $C_{Aliph}H_2$), 3.32(s, 8H, N-CH_2), 5.72(s, 8H, N-CH_2), 7.86(s, 8H, Ar-H). ^{13}C NMR (110 MHz, DMSO–d_6, δppm), 14.1(4C, CH_3), 51.0(4C, N-CH_2), 113.0, 125.0, 128.0, 135.0 (28C, Ar-C), 185.0 (4C, N_2C-Ag). ESI-MS (m/z):$[M-2]^+$ Cal. for $[C_{75}H_{99}Ag_2N_8]^+$ = 1342.35 Da, Found 1342.25 Da. HPLC purity: 98.18%. Ana. Cal. for $[C_{75}H_{101}Ag_2N_8]^+$: C 55.82; H 6.41; Ag 13.19; F 13.94; N 6.85; P 3.79. Found: C 55.80; H 6.40; N 6.80.

2.7. 1,4-bis((3-decyl-2,3-dihydrobenzimidazol-1-yl)methyl)benzene, silver hexafluoro phosphate (*C3*)

L3 (0.8 g, 1.02 mmol) and Ag_2O (0.47 g, 2.05 mmol) were dissolved in 100 mL of methanol was reacted for 20 h by following the same procedure as used for **C1.** Light gray powder was obtained. Yield: 75%. M.P 189.3 °C. UV–vis (λ^{max}, nm): 270.00, 290.00 (π-π*and n-π*), 300.00 (LMCT). FLR emission (λ^{max}, nm) 345.0 303 nm. FTIR (ATR cm^{-1}): 2924, 2853 (C—H strch), 1478 (C-Ag strch), 1342 (C—N strch), 791, 743 (C— H bend). ^{1}H NMR (400 MHz $DMSO_{d6}$, δppm), 1.32(t, 40H, $C_{alip}H_2$), 1.67(m, 8H, C_{Aliph}-H_2), 3.14(m, 8H, N-CH_2), 6.36(s, 8H, Ar-H). ^{13}C NMR (110 MHz, $DMSO_{d6}$, δppm), 14.1(4C, CH_3), 51.0, 52.0(4C, N-CH_2), 113.0, 125.0, 128.0, 135.0, 138.0(28C, Ar-C), 185.0(4C, N_2C-Ag). ESI-MS (m/z): $[M + 1]^+$ Calc.for $[C_{84}H_{125}Ag_2N_8]^+$ = 1460.90 Da, Found 1461.08 Da. HPLC purity: 99.04%. Ana. Cal. for $[C_{84}H_{124}Ag_2N_8]$: C 57.73; H 6.92; Ag 12.34; F 13.05; N 6.41; P 3.54. Found: C 57.70; H 6.90; N 6.40.

2.8. Computational details

SCIGRESS software has been used to optimize the structure of the new complexes (**C1**-**C3**), [16]. The vibrational frequency optimized geometrical parameters and molecular chemical properties were carried out using the Mechanics method with MO-G-PM6 level. The biological activities of the optimized complexes (**C1**-**C3**) were done using Discovery Studio (DS) 3.5 [17]. The binding affinity of the docked molecules with DNA (PDB ID: 1BNA), BSA (PDB ID: 3 V03) and cancerous protein targets such as Bruton's tyrosine kinase (PDB ID: 3PIY), human topoisomerase II alpha (PDB ID: 4FM9) and aromatase cytochrome P450 (PDB ID: 3EQM) can be predicted and observed efficiently with molecular docking analysis. Molecular docking simulation was performed by AutoDock Vina software [18,19]. The crystal structure of DNA and the current proteins were obtained from Protein Data Bank (PDB)[20]. The respective targets were prepared by removing co-crystalline ligand and water molecules and polar hydrogen was inserted to the respective targets and protein ionization and residue pKs were computed by CHARMm [21]forcefield with the support of the sub-protocols of DS 3.5. The title complexes which were minimized at the MO-G-PM6 basis method is used as the ligands. The binding site(s) of the targets were determined based on DS 3.5 tool and the literatures. Finally, the docking processes were applied between ligand(s) and target(s). The final images of the potential docked complexes were analyzed using UCSF Chimera [22]and Discovery Studio 3.5[17]. The interpretation of molecular docking calculations for each target can be evaluated by the binding energy, root-mean-square deviation (RMSD < 2.0 Å) values and non-bonding interactions estimated from the docked poses of the complexes (**C1-C3**).

2.9. Stability assay

Stability in solution form of synthesized complexes **C1-C3** was determined by scanning spectral behavior through uv spectroscopy and HPLC-DAD for a definite time zone. Synthesized candidates were dissolved in minimum possible concentration and were diluted further to 10^{-4} M with phosphate buffer solution (PBS) and their spectras were scanned over 7 days respectively, by following the approach of [23]. HPLC-DAD was used to monitor area under curve for each drug.

2.10. Lipophilicity

Lipophilicity of synthesized complexes in terms of log P and log D was monitored through ability of distribution of test compounds between aqueous and organic (*n*-octanol) layers. UV–Vis spectroscopy was used to determine the concentration of these compounds in each phase. Log P and log D values were determined through logarithmic ratio of concentration between these two phases by following equation.

(Log P = Log ([org]/[Aq]).
(Log D = Log([org]/[Aq]).

2.11. Biomolecule interaction studies

The synthesized compounds were studied to probe their potential interaction with CT-DNA (Calf thymus DNA) through spectroscopy as per Gaber, et al. [24] methodology. Briefly, stock solution of CT-DNA was prepared by dissolving appropriate amount of CT-DNA (0.051 g) in 50 mL of Tris-buffer of pH 7.4 (Tris-HCl, 10 mM) and stored for 24 h. Further dilution of this stock solution in the same buffer was prepared of concentration adjust through spectrophotometer to meet the ratio of 1.9 (optical density at 260 and 280 nm respectively). Test solutions were prepared for various concentrations of sample (0.01 mM-0.1 mM) but fixed concentration of CT-DNA and analyzed for their spectroscopic behavior. The affinity among samples and ct-DNA was estimated in terms of binding constant Kb by noting spectral changes and regression analysis of concentration verses response through Equation given below.

$[DNA]\ \epsilon_a - \epsilon_f = [DNA]\ (\epsilon_b - \epsilon_f) + 1/(\epsilon_b - \epsilon_f)$.Where ϵa is [abs/M], ϵb and ϵf are extinction coefficients in presence and absence of DNA of test compounds respectively.

FTIR spectroscopy was also employed for investigation of potential binding intensity as well DNA interaction mechanism. The prominent spectral shifts in transmission frequencies of IR spectra upon interaction of DNA with metal complexes could be lead understanding of binding pattern or binding nature.

viscosity measurements of test solutions (test compounds and CT-DNA mixture) and CT-DNA pure solution, were made on Ostwald micro-viscometer at maintained temperature 27 °C [25]. The concentration of CT-DNA was fixed while concentration of

complexes C1-C3 varied to give R (R = [complex]/ [DNA]) from 0.01 to 0.50. The results were plotted as relationship of R versus $(\eta/\eta 0)^{1/3}$, where η are the specific viscosity of test solutions and η_0 is specific viscosity of DNA solution. The relative values of η and η_0 were obtained by following the equation.

$$\eta/\eta_0 = (t_{complex\ solution} - t_0)/t_0/(t_{CT} - DNA - t_0)/t_0$$

here, t_0 is the time of buffer solution.

Interaction with BSA: UV–visible spectroscopy was used to probe the interaction of synthesized complexes with BSA at increasing concentration of sample while fixed concentration of BSA (0.01 mM) [26]. Spectral behavior shift and absorption pattern was noted which help in predicting binding constant as well as binding pattern of drug with BSA.

Hemolytic Assay: Hemolysis to red blood cells (RBCs) by test compounds (**C1**-**C3**) was studied by monitoring the damaging rate of RBCs through spectroscopic approach [10]. Results were compared with standard drug Triton-X as positive control.

2.12. Cytotoxicity assay

Cytotoxicity measurements of synthesized compounds was made against selected cancerous strains through MTT assay by following optical density approach [27]. This assay based on principle that unreacted amount of formazan product reflects the proportion of live cells and rest portion is of dead cells. Synthesized complexes (**C1**- **C3**) and salts (**L1**-**L3**) were prepared for series dilution (0.01–10 μg mL^{-1}) in DMSO and the reference drugs like oxaliplatin, cisplatin and 5-Florouracil (0.0001–1 μg mL^{-1}) were also prepared as positive control. Human lung cancerous strain A549 (1000 cell/well),breast cancerous MCF-7 (1000 cell/well), HeLa cells (1000 cell/well) and colon cancerous strain HCT 116 (1000 cell/well) were cultured separately in DMEM medium (Dubecco's modified Eagle medium) in continuous aeration of 5% CO_2 and added 100 μL medium in 96 well plates and incubated at 37 °C for 24 h [28]. After an interval of 24 h, DMEM was replaced with freshly developed DMEM and 10 μL of each sample of every concentration separately was added. For the accurate results, treatments were repeated thrice. Control was monitored to grow cell lines without any treatment with the therapeutic agents hold up living cells only in well plates and blank DMEM in triplicate was also monitored on multi-plate reader. After 48 h of incubation, a measured amount of 20 μL of MTT dye (5 mg/ml in PBS) was poured to each well and further incubate for 4 h at 37 °C. Product of wells were drained and frozen product was dissolved in 100 μL DMSO until, showed purple color. Biobase multiplate reader through Gen 2.0 was accessed to measure the absorbance of each well at 570 nm and % viability of cells was determined by following formula.

$$\%\ cell\ viability = ODsmp/ODcontrol \times 100$$

OD is optical density at 570 nm.

2.13. Cell cycle analysis

Cell cycle analysis is a technique to estimate the DNA content in cells through propidium iodide used as florescent dye which enters cells having ruptured membranes after treatment with cytotoxic compound. Propidium iodide can bind to any type of genetic material either it is nuclear DNA, RNA or mitochondrial DNA. Mitochondrial DNA has negligible amount in cytosol. To obtain just nuclear DNA in cells RNase is added to break RNA so that PI only binds to DNA. This univariate analysis helps to obtain the phase at which cell cycle arrest can be caused by certain molecule. The difference of DNA content in G0/G1 phase S (Synthesis), and G2/M can be estimated by this univariate analysis [29]. The most effective cytotoxic derivatives were selected for flow cytometry analysis.

For the assessment of apoptosis cell cycle analysis was carried out by flow cytometry using previously mentioned procedure [30].To perform cell cycle analysis, cells were planted in a population density of $3x10^5$ cells per well and incubated for 24 h in a CO_2 incubator at 37 °C. Most potent samples were selected from the series and placed on 10 μM and 20 μM concentrations. Cells were harvested in the appropriate manner and centrifuged at 3000RPM for 5 min and washed with PBS. Cells were fixed using 70% ethanol drop wise on continuous vortex to lessen agglutination during fixation. After fixation cells were placed in −20 °C for 1–2 h. After complete cell fixation again centrifugation was done to collect cells pellet. Then pellet was suspended with propidium iodide (PI) solution (20μg/ml), 0.1% (v/v) triton X-100, RNase 50μg/mL. Samples were placed in dark for 30 min. Then samples were run using BD Accuri C6 flow cytometer and 10,000 events were taken. The obtained data was analyzed by using BD Accuri™ C6 software and GraphPad Prism 5.01.

2.14. Microscopic analysis of apoptosis and ROS generation assay

The microscopic assessment of most potent samples was performed in parallel to flow cytometric analysis. The investigation was carried out as reported previously [29]. The ROS production in HeLa cells and MCF-7 cells was assessed by fluorescence microscope. Cells were grown in 24 well plate on coverslips treated with 30 μM and 60 μM end concentration of the complex. After 24 h, cells were treated with dichlorofluorescin diacetate (H2DCF-DA) dye, and reaction mixture placed in the absence of light for 10 min, and observed under fluorescence microscope as previously reported [29].

3. Results and discussion

3.1. Optimized geometry and HOMO-LUMO analysis

The related compounds were minimized at MO-G/PM6 level of SCIGRESS and their xyz coordinates of optimized geometry is provided in supplementary data, Table S2-S4. HOMO and LUMO energy is considered a key property that reflects chemical stability and reactivity of the molecules. The HOMO-LUMO properties for complex (**C1-C3**) were calculated by using earlier said software. Then, the numerical energy values of the HOMO and LUMO orbitals were used to predict their stability and reactivity. Fig. 1 shows the images of the HOMO-LUMO orbitals for the compounds (**C1-C3**). The LUMO orbitals of each complex are located in the imidazole part of molecules as remarked by the yellow and red colors, while their HOMO orbitals (as indicated blue and green color) are located mostly in the Ag metal(s) and to a lesser extent in other parts of the molecule. It is well established that HOMO-LUMO energy gap (ΔE) expresses the charge transfer interface within the molecules. The E_{HOMO}, E_{LUMO}, and energy gap of each compound were shown in Fig. 1. The results revealed that compound **C1** (5.20 eV) had higher reactivity, greater polarizability, and lower stability; So that the charge transfer of the molecular frontier orbitals in the compounds **C1** happens more easily than others (**C2** and **C3**).

3.2. Synthesis and characterization

Synthesis of precursor (**I**), azolium salts (**L1**-**L3**) and silver complexes (**C1**-**C3**) was accomplished by following the approach of [8] mentioned in Scheme 1. Initially, synthesis of precursor-I was carried out in first step by *N*-alkylation (N1) at terminal nitrogen of benzimidazole in basic media by reacting with 1,4-dibromo-p-

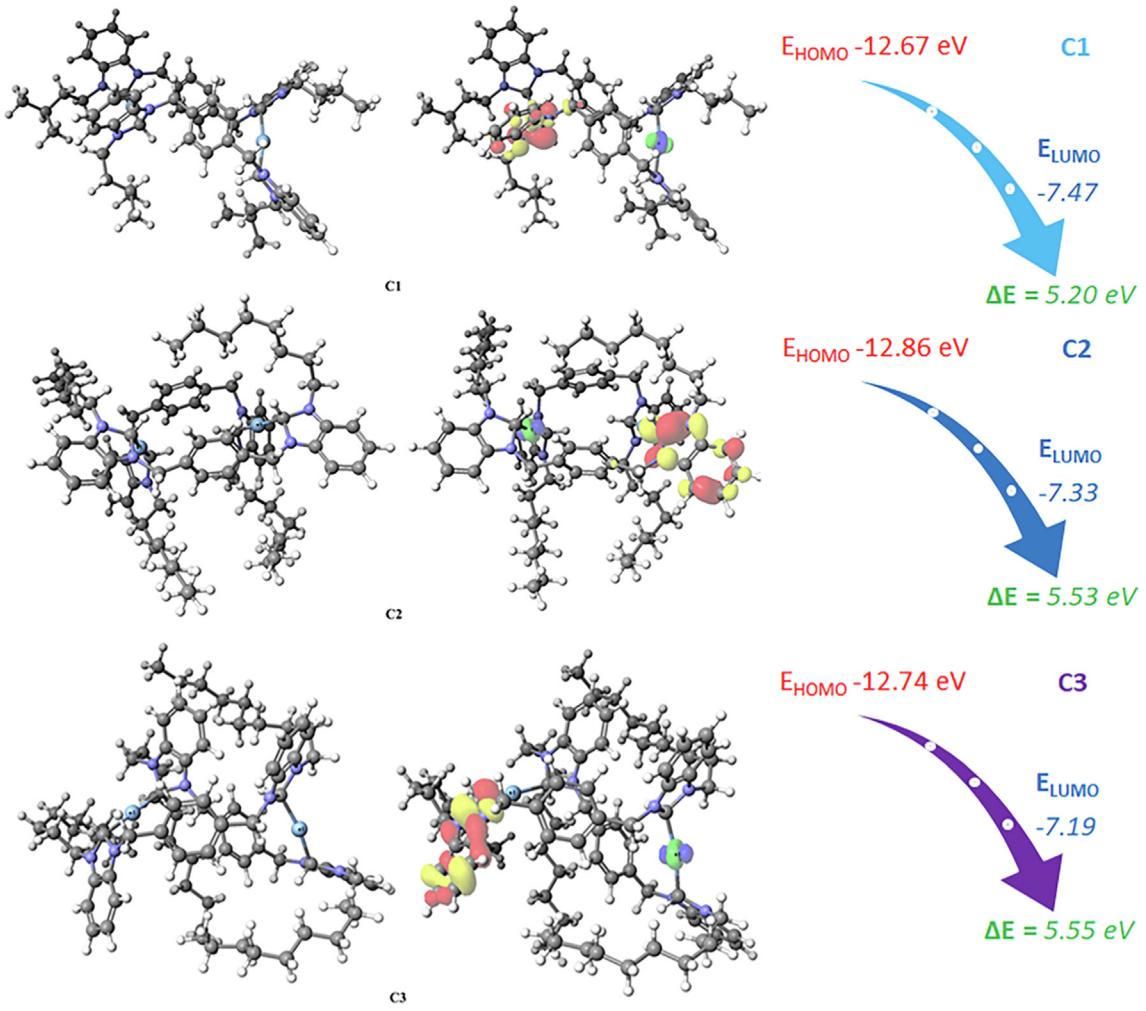

Fig. 1. The optimized structures and HOMO (blue-green lopes) LUMO (red-yellow lopes) molecular orbitals, molecular properties and values calculated from the HOMO and LUMO orbitals of the related compounds (**C1**-**C3**). (For interpretation of the references to color in this figure legend, the reader is referred to the web version of this article.)

xylene. In the second step, the alkylation on second nitrogen (N2) of the precursor was done by refluxing (24 h) precursor (**I**) with 2-methylbutyl bromide, 1-bromo octane and 1-bromo decane separately in 1,4-dioxane which results (**L1**-**L3**) respectively. Synthesized salts (**L1**-**L3**) were further proceeded for silver metalation through reaction with Ag_2O in absence of light for 48 h (at room temperature) to produce silver complexes (**C1**-**C3**) by following the method of [8] Scheme 1.

DMSO solution of precursor (**I**), salts (**L1**-**L3**) and silver candidates (**C1**-**C3**) were studied through UV–vis spectrocopy to observe any shift in spectral behavior [31,32]. Interestingly (**L1**-**L3**) showed bathochromic shift from spectral behavior of Precursor-I that could be an indication of conversion of precursor to respective ligands through structural modifications [32]. While studying silver adducts (**C1**-**C3**) red shift was observed (**Fig. S1**) that could be due to ligand to metal charge transfer (LMCT) [31] and partial covalent nature confined to MC (metal centered bands). HOMO and LUMO picture from DFT measurements of complexes **C1, C2** and **C3** also showed the maximum electron density on ligands orbital, which contributes in electronic transition from n → π^* or π → π^* in optimized structures [33]. Similar trend in shift of absorption pattern corresponds to coordination of metal center to molten salts was reported in literature [8]. Synthesized compounds were further confirmed through emission spectroscopy in acetonitrile solution at room temperature and results are presented in supplementary data (**Fig. S2-S3**). Synthesized silver complexes showed blue shift in emission spectra from their respective ligands (**L1**-**L3**) when studied in the range of 220–500 nm at excitation wavelength 380 nm. This shift in emission pattern could be an indication of ligands transformation to silver candidates.

FTIR spectroscopy also assured formation of precursor, ligands and confirmed their transformation into silver complexes (**C1**-**C3**). An intense absorption pattern observed for (**L1**-**L3**) in the range of 3050–2900 cm^{-1} (absent in Precursor-I) could be due to substitution at **N2** position of Precursor-I (Fig. S4) that confirmed successful transformation of (I) into ligands (**L1**-**L3**) [34]. An intense distinguished four finger pattern in the range of 1456–1400 cm^{-1} for compound (**C1**-**C3**) is an indication of successful conversion of ligands (**L1**-**L3**) into respective silver complexes (**C1**-**C3**) [35]. Structural confirmation of synthesized compounds was assured through ^{1}H NMR spectroscopy of which detailed results are described in experimental section. Characteristic peak for azolium salts appeared at 9.95–10.57 ppm are resonance of carbene protons (NCHN) which confirmed the successful formation of (**L1**-**L3**) from Precursor-I (**Fig. S5-S11**). The appearance of peculiar pattern of NCHN is a characteristics of formation of benzimidazolium salts [9,36–38]. Interestingly, the resonance peak of NCHN disappeared for candidates (**C1**-**C3**), an indication of carbene proton replacement with metal center to produce silver complex [39], and this interesting phenomenon is presented in supplemen-

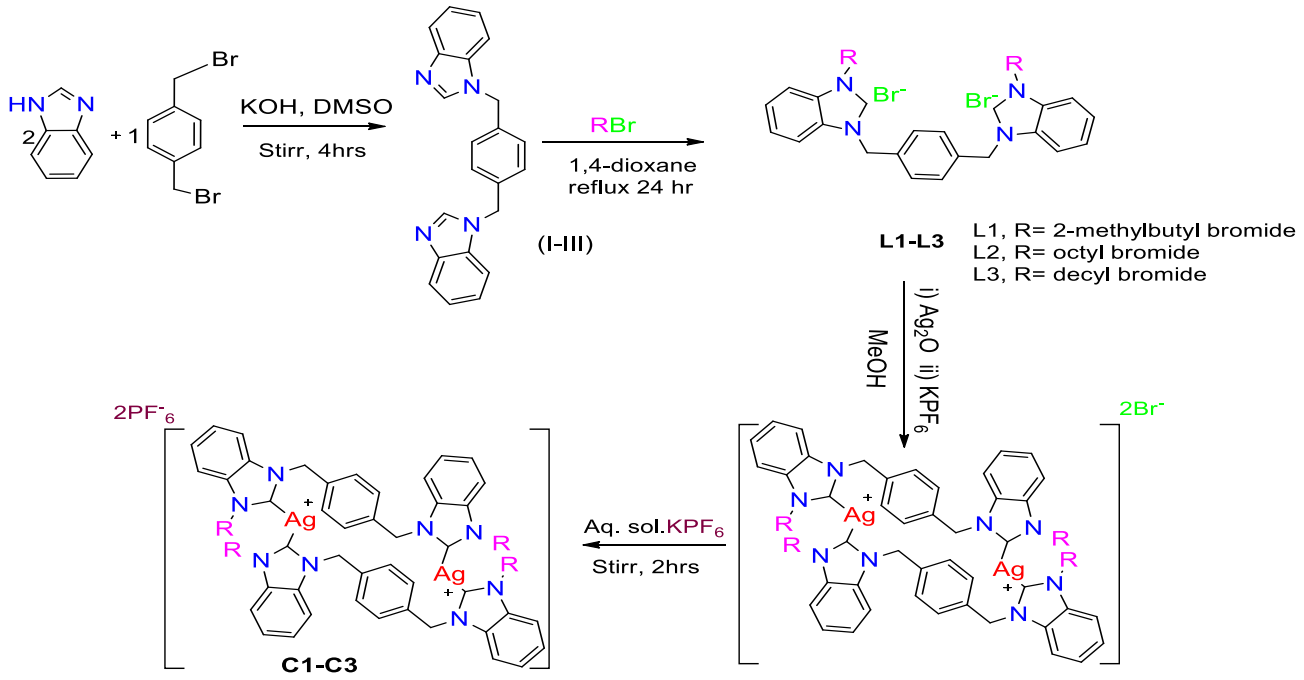

Scheme 1. Synthesis of precursor (**I**), salts (**L1-L3**) and their silver complexes (**C1-C3**).

tary material (**Fig. S5-S11**). Our claim of Successful synthesis of salts (**L1-L3**) was further assured through ^{13}C NMR spectra where a prominent peak at 144–151 ppm is associated to carbene carbon (NCN), supplementary data (**Fig. S12-S18**) which is in line agreement with literature that reports chemical shift (^{13}C, ppm) for their compounds at 142.6, 143.0 ppm [9,40] and 142.1, 144.7, [41] for carbene carbon (NCN) of azolium salts. This characteristic pattern was shifted to the low field (178.8–185.0 ppm) for complexes (**C1-C3**), which is an indication of change in environment of carbene carbon for the synthesis of silver candidates, detailed NMR spectra is given in supplementary data (**Fig. S5-S18**) and description is given in experimental section.

Synthesized compounds were further confirmed by electron spray ionization mass spectrometry (ESI-MS). The ESI-MS spectra was obtained in both positive as well negative ion mode by injecting the sample directly into the mass spectrograph and observed the parent ion peak as well as fragmentation pattern and compared with the theoretical spectra studied through chemdraw ultra pack 12.0 [9,38]. Interestingly, spectral findings of mass spectrum for all studied compounds found corresponds to theoretical values and confirmed the successful synthesis of designed compounds; details are described in Materials & methods section and supplementary data **Fig. S19-S25**.

3.3. Stability assay

One of the most dominant concern in drug development especially for organometallic candidates is their stability which affects its bioavailability as well as efficacy at target site. Stability profile of related compounds (**C1-C3**) was studied through UV–visible spectrophotometer by monitoring spectral behavior for specific time period (0–7 days) and interestingly a repeatable pattern was observed for all compounds that is an indication of stability in solution form. This stability was further confirmed through chromatography for any possible degradation by using reverse phase high performance liquid chromatography (RP-HPLC-DAD) by monitoring the area under the curve as well as retention time for seven consecutive days and results are presented in supplementary data (**Fig. S26-S32**) Time depending (**1–7** days) chromatograms of solution (0.1 mg mL^{-1}) showed no observable change in area under curve as well in chromatographic and spectral behavior over evaluation time, supplementary data (**Fig. S26-S32**). This repetition in behavior without any change in spectral or chromatographic pattern over the studied period indicates the stability of test compounds in solution form [9].

3.4. Molecular docking studies

Molecular docking is in silico visualization methods, carried out to estimate the binding potential of studied compounds with biological targets (DNA and BSA) and in various protein targets to elucidate their possible biological activity on cancer cell proteins molecular basis. Molecular docking studies of compound (**C1-C3**) were applied against various cancer proteins (leukemia, colon and breast) to find their best modes and non-bonding interactions with these targets and results are shown in supplementary data (**Fig. S33-S36**). Simulative calculations provided lowest binding energy values of each compound which is graphically presented in (Fig. 2 **(C)**. Besides, detailed information for the interaction types and distances of the three compounds with the target models are listed in supplementary data (**Table S1**).

When compounds were investigated against DNA nucleotides, the binding pose of **C1** displayed a binding energy of – 7.51 kcal/mol. The compound **C1** forming three H-bonds with the nucleotides, B: DT19, A: DC9, and B: DT20. In addition, the benzene linkers form two electrostatic interactions with nucleotides B: DT20 and B: DC21. The alkyl group of current compound was engaged hydrophobically in three interactions with the nucleotides A: DA6, A: DT7 and B: DT20 (supplementary data **Fig. S33-S36**). On the other side, the compound **C2** made four H-bonds with A: DG10, A:DC9, B:DA18 and B:DT19; two electrostatic interactions with A:DG10 and A:DC11, and also four hydrophobic interactions with A:DG10, A:DC11 and B:DG16 nucleotides of DNA in supplementary data (**Fig. S33-S36**) and (**Table S1**). Although compound **C2** interacts better with DNA than compound **C1**, the compound **C1** dominates in terms of thermodynamic binding affinity than

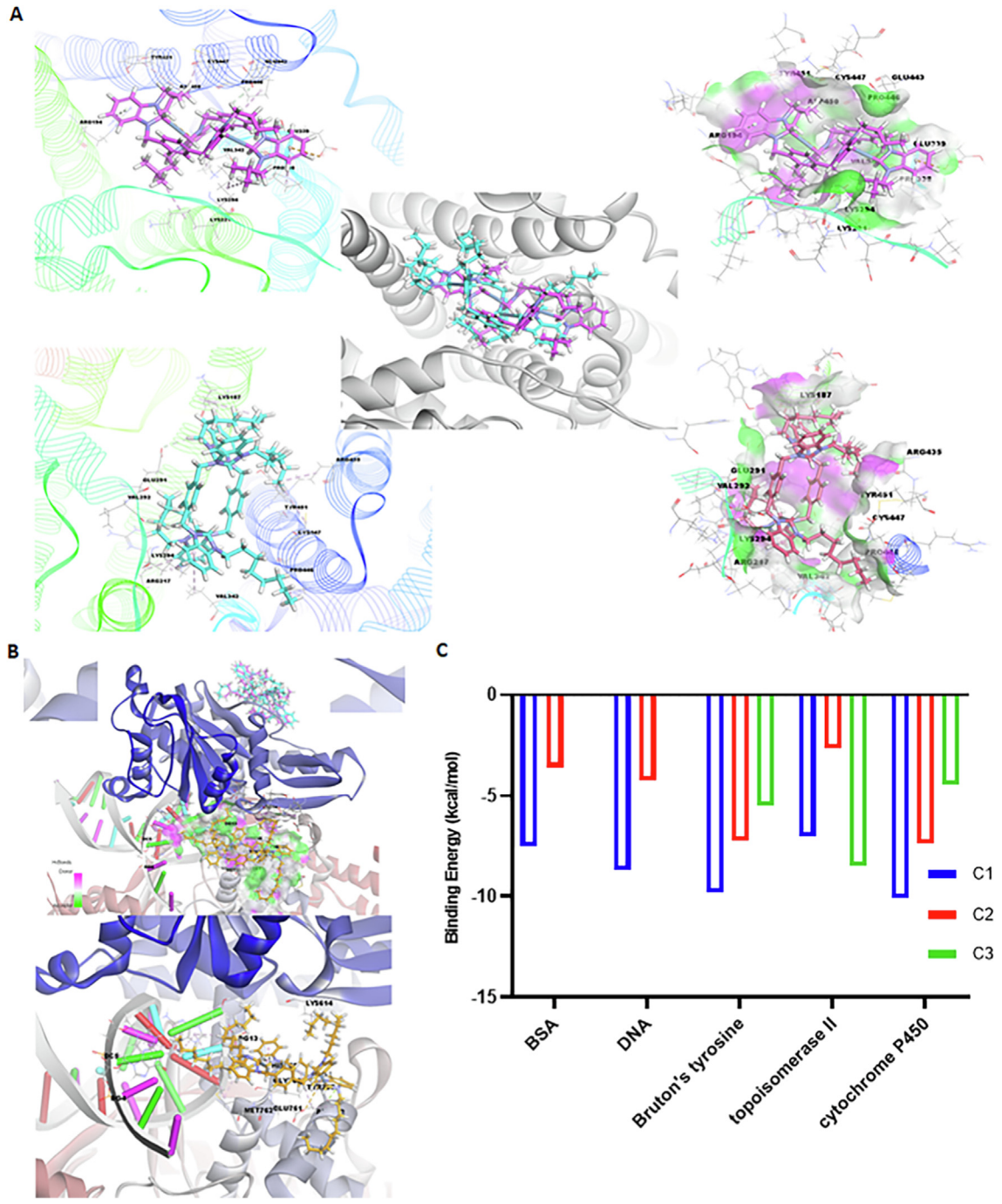

Fig. 2. **A**) **3D** views of interactions of each complex (**C1**, pink, stick; **C2**, cyan, stick) against BSA and surface mapping of hydrogen bond donor/acceptor surface on **BSA**. **B**) **3D** views of interactions of each complex (**C1**, pink, stick and **C2**, cyan, stick) against human topoisomerase **II** alpha and surface mapping of hydrogen bond donor/acceptor surface on Human topoisomerase II alpha. **C**) Binding energy values of the compounds, (**C1, C2** and **C3**) with DNA, BSA and various cancer proteins (leukemia, colon and breast). (For interpretation of the references to color in this figure legend, the reader is referred to the web version of this article.)

the compound **C2** in the active site of the target, as seen in (Fig. 2)**.** Beside these, compound **C3** shows no interaction with the same target due to its steric nature.

When the interaction of the same compounds (**C1**-**C3**) with the BSA target is examined by molecular docking method this time, it is seen that the compound **C1** has a predominantly better binding tendency than the other **C2** and **C3** compounds. This situation is illustrated in (Fig. 2 (**C**). Compound **C1** has three hydrogen bonds (Pro338, Glu443, and Arg194), two electrostatic interactions (Glu339 and Asp450) and eight hydrophobic interactions (Cys447, Lys221, Lys294, Tyr451, Pro446, Val342 and Pro338) with the BSA target, while the compound **C2** has hydrogen bonds with the amino acids Val292 and Glu291; and also hydrophobic interaction with Lys187, Arg435, Cys447, Pro446, Tyr451, Lys187, Arg217, Val432 and Lys294 of the same target (Fig. 2 and supplementary data **Table S1**). The last compound **C3** did not interact with the BSA target as in DNA. Compounds **C1** and **C2** exhibited different binding poses and at different locations within the active region of the target structure. The interaction pose of the compound **C1** structure, the binding energy value of −7.51 kcal/mol and the

interaction types showed more potential dominance than the other compounds.

In addition to their relevance to DNA and BSA, the investigation of whether they can show on various anticancer targets has been tried to be estimated by molecular docking application. First, the calculations for Bruton's tyrosine kinase target have the best binding affinity for **C1** (-9.78 kcal/mol)**, C2** (-7.21 kcal/mol) and **C3** (-5.51 kcal/mol), respectively. It is observed in **Table S1** that the binding affinity here exhibits a better binding affinity than the previously evaluated DNA and BSA targets. Considering each compound target at the atomic level, compound **C1** is predominantly hydrophobic interaction alongside hydrogen bonding with the target enzyme. Compound **C2**, on the other hand, exhibits a completely hydrophobic interaction with the same target enzyme, as well as in a different region from compound **C1**, as seen in supplementary data (**Fig. S33-S36**). As the last compound, the compound **C3** creates a hydrophobic interaction with the target in a region similar to the compound **C2** and also makes electrostatic interaction and hydrogen bonds with the target enzyme.

Then, when the relationship between the related compounds with the Human topoisomerase II alpha target is investigated, unlike the other targets, the compound **C3** exhibits the best binding tendency with the target enzyme with a binding energy value of −8.49 kcal/mol. The compound **C1** is in second place with a binding energy value of −7.01 kcal/mol. Finally, the compound with the lowest binding affinity with a value of −2.64 kcal/mol is **C2**. The reason for these situations is that the compound **C3** exhibits strong non-bonding interactions with both the enzyme and DNA. The other two compounds interact only with the enzyme, as indicated in (Fig. 2), and they interact in a different region of the target enzyme than the compound **C3.**

Molecular docking was performed to obtain information about the binding affinity and interaction mechanisms of the three recently mentioned compounds with the Aromatase cytochrome P450 target. As a result of the calculation data obtained, the lowest binding energy value is observed as compound **C1** of −10.05 kcal/mol. Afterwards, the compounds **C2** and **C3** follow. When we focus on the interactions of target enzyme-related compounds, compound **C1** exhibits electrostatic interaction and hydrogen bonding with Glu357 and hydrophobic interactions with Tyr424 and Tyr441 amino acids of the target model. Compound **C2**, like compound **C1**, creates electrostatic interaction and predominantly hydrophobic interaction with the target enzyme, except for hydrogen bonding. The last compound, **C3**, has the lowest binding affinity with the target enzyme, although it creates strong hydrogen bonding with Tyr441 and hydrophobic interactions in a different region as seen in supplementary data (**Fig. S33-S36**). The compound **C1** considered as a result of interactions with different target models, have a potential inhibitory feature on the basis of both chemical and in silico calculations.

3.5. Lipophilic assay

Lipophilicity is one of the important characteristics for drug design specified by Lipinski's approach, it helps in determining the ability of the therapeutic agents to cross cell barrier and drug ability. Distribution coefficient values also assist in determining the lipophilic character, greater the Log D value more the drug will distribute itself into the polar solvent like water and less will be the potential to cross the cell barrier. The lipophilic behavior of silver candidates (**C1**-**C3**) was observed through flask shake method and the results of log P are given in (Table 1). Lipophilic values of silver candidates (**C1**-**C3**) were found in the range from 0.898 to 0.942. More the aromaticity less will be the Log P value and more readily it will cross the cell barrier [10]. Complex **C1** has less Log P as well Log D value than the other studied complexes **C2** and **C3**, so more potent it is to cross the cell barrier. This ability of complex to cross cell barrier may be due to the coordination behavior, ligand bond polarity, and metal coordiantion through charge equilibrium[42–48]. The lipophilic values of studied silver candidates showed that it lies in best criteria of the good lipophilic character. Among the studied candidates the diversity in lipophilic values is confined to the structrual modifications at azolium and moiety [9]. The previously reported literature suggested that cytotoxicity and the ability to cross the cell barrier is lipophilicity dependent phenomenone [23].

Table 1
Lipophilic values of compounds (**C1**–**C3**).

Sample	C_o	C_w	Log P
C1	9.89	1.25	0.898
C2	9.32	1.12	0.920
C3	8.59	0.98	0.942

C_o is concentration of analyte in organic phase, C_w is concentration of analyte in aqueous phase.

3.6. Cytotoxicity and hemolytic assay

The synthesized complexes (**C1**-**C3**) as well their salts (**L1**-**L3**) were studied for their cytotoxicity profile against four different carcinoma cell lines (MCF-7, A549, HCT-116 and HeLa) by MTT assay. Susceptibility to cancer strains of studied compounds (**L1**-**L3**) and (**C1**-**C3**) (0.05 mg mL^{-1} of each compound) was determined against two cell lines, MCF-7 and HeLa cell lines, and compared with standard drugs cisplatin and 5-FU, results are presented as bar graph in Fig. 3. Interestingly, compounds (**C1**-**C3**) showed far superior activity than that of salts (**L1**-**L3**) which was a lead for extensive study of screened compounds against other cell lines at various concentrations. Our observations of better activity of silver complexes (**C1**-**C3**) from their precursor ligands (**L1**-**L3**) might be due to the contribution of the silver center and its bioavailability [28,49,50]. Screened compounds (**C1**-**C3**) were further investigated for dose dependent response (0.001–10 μg mL^{-1}) against four cancer strains and results are presented in (Fig. 3**)**. Results showed that cytotoxicity increased with gradual increase in concentration and a direct relationship was observed which indicates that Cell viability is a concentration dependent phenomenone [9]. The IC_{50} values of test compounds (**C1**-**C3**) showed cell selective toxicity. The test compounds were found more potent against MCF-7 having IC_{50} 6.28 ± 0.82–9.55 ± 0.71 μM than standard drug 5-FU (IC_{50} 12.87 ± 1.0 μM) [14]. Order of cytotoxicity of test compounds for MCF-7 and HeLa cell lines (**C1** > **C2** > **C3**) while for A549 (**C1** > **C3** > **C2**) (Table 2).

Cytotoxicity of designed compounds can be predicted through computational calculations especially, HOMO-LUMO energy gap that have vital role to determine the cytotoxicity and lipophilic character of the test compounds. Simulation calculations predicts low HOMO-LUMO energy gap for test compounds which inclined to higher reactivity and greater polarizability. In addition, molecular frontier orbitals in the compounds **C1** happens more easily than **C2** and **C3** and leads to greater lipophilic character and better biological activities. Cytotoxicity of test compounds was relatable with hydrophobic character and found a direct relationship among cytotoxicity and hydrophobicity [51,52]. A general trend from literature was observed that cytotoxicity increases through increase in hydrophobicity as witnessed by [53,54], Hence, Complex **C3** is least in hydrophobicity and thus showed least cytotoxic effect. However, these complexes (**C1**-**C3**) showed an increase in cytotoxic effect with the increase in hydrophobicity among them **C1** showed an exceptional behavior with IC_{50} value (6.28 ± 0.82) with logP 0.898. Results showed that hydrophobic factor which is responsi-

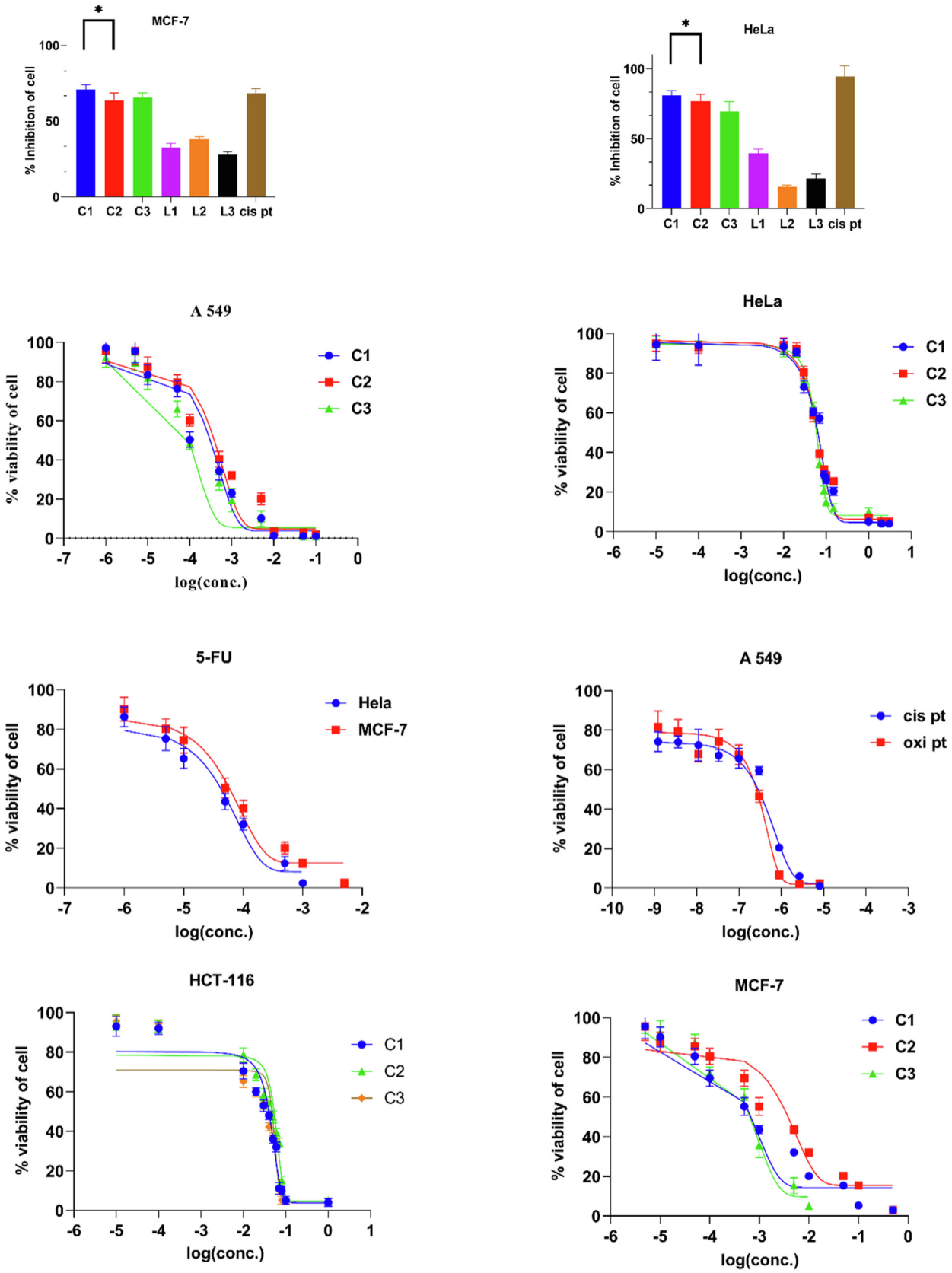

Fig. 3. Results of cell viability of (**L1**-**L3**) and (**C1**-**C3**) by MTT assessed at 100 μM concentration on HeLa and MCF-7 cell line while concentration dependent response of **C1**-**C3** (1 mM-1 μM) and standard drugs cisplatin (cis pt), oxaliplatin (oxi pt) and Flourouracil (FU) against HeLa, MCF-7, HCT-116 and A549 cell lines.

Table 2
Minimum inhibitory concentration IC_{50} of (**C1**-**C3**).

	IC_{50} μM			
	MCF-7	HeLa	A549	HCT-116
C1	6.28 ± 0.82	10.54 ± 0.85	9.17 ± 0.60	14.32 ± 1.0
C2	8.15 ± 0.65	14.36 ± 1.0	13.54 ± 0.55	12.54 ± 1.0
C3	9.55 ± 0.71	15.36 ± 0.55	12.87 ± 0.80	16.35 ± 1.2
cis pt	8.74 ± 0.52	11.35 ± 0.50	13.82 ± 1.0	–
5-FU	12.87 ± 1.0	15.47 ± 0.62	14.36 ± 0.75	18.65 ± 1.5

Experiment was conducted in triplicate and presented as Mean ± SD.

ble for the drug to cross the cell barrier and contributes in bioavailability at the target site had direct effect on cytotoxicity of silver complexes [51,53,55]. Although all complexes have better potential but Complex **C1** was found to be more cytotoxic against MCF-7 strain with least (**IC_{50}** 6.28–9.55 μM) value, and show even better potential than reported complexes with (**IC_{50}** > 20 μM) [37] and standard drug 5-FU (**IC_{50}** 12.87 ± 1.0 μM [8,56]. Test compounds (**C1**-**C3)** against red blood cells (RBCs) were investigated for hemolysis activity through spectroscopy and results compared with positive control (Triton X). It was investigated that all studied complexes were found harmless to RBCs than Triton X positive control. Studied complexes (**C1**-**C3**) showed %hemolysis in the range of 7.6–10.8% while Triton X showed 92.9%. The low hemolytic activity of test compounds showed that studied compounds are innocuous for RBCs while pernicious for cancerous cells.

3.7. Microscopic analysis of apoptosis and ROS generation assay

Studied compounds showed good anticancer potential studied through MTT assay and among them, most active compound was further probed through microscopic analysis and ROS generations assay. The loss of nuclear integrity and induction of nuclear fragmentation on HeLa and MCF-7 cell lines treated by related compounds was confirmed by DAPI (blue florescent DNA labeling dye) staining technique and results were visualized through fluorescent microscopy. Interestingly, clear morphological changes were observed in treated cells than that of control (DMSO treated) in microscopic images. Fluorescent microscopy images of HeLa cells and MCF-7 cells treated with **C1** (30 μM and 60 μM) and DMSO treated cells (control) are presented in (Fig. 4) where an increased blue fluorescence is evident for complex treated cells as compared to control. Furthermore, morphological changes associated with apoptosis like nuclear fragmentation, and chromatin condensation are very evident in the cells upon treatment (Fig. 4) (**A** & **A1**). Compounds were found more active against HeLa cells than MCF-7 because better nuclear shrinkage and disappearance of fluorescent strains were observed in earlier that were barely observed in control, a clear indication of apoptosis. PI staining was also performed to distinguish among live and dead cells because PI dye enters into ruptured membrane dead cells emitting red fluorescence wing to Förster resonance energy transfer (FRET) that indicates about cell integrity [57]. Complex treated HeLa cells and MCF-7 cells showed progress growth of PI staining positive cells while treating with two separate concentrations (30 & 60 μM). Chromatin condensation and nuclear fragmentation for the formation of apoptotic bodies are clearly visible in Fig. 4 (**B**&**B1**) after PI staining of C1 treated HeLa and MCF-7 cells respectively.

Moreover, treated cancer cells were also stained with DCFH-DA dye to investigate any possible ROS generation which can subsequently cause damage to functional biomolecules (DNA, RNA, protein etc.) and results in cytotoxicity. Interestingly, studied compounds showed significant increase in ROS production in both HeLa and MCF-7 cells lines at concentrations 30 & 60 μM in comparison to control (Fig. 4 **C&C1**) when cells were visualized by fluorescence microscope (Nikon ECLIPSE Ni–U with the magnification of 20X). The treated cells showed fluorescent behavior of disintegrated cellular membrane and condensed cellular protein that could be due to oxidation of proteins and lipids. Similar finding was reported by [58] against HeLa cell lines which exhibited fluorescent behavior owing to production of ROS.

To further probe the cytotoxic mechanism of studied compounds, cell cycle arrest analysis for **C1** compound was carried out to measure the mitochondrial DNA contents with PI staining. Although DNA has small amount in cytosol and PI staining is not particular for DNA therefore, RNase was used to deactivate RNA contents in the cell[59]. A difference in DNA contents, G_0/1 (gap zero and gap one), G_2/M (gap two and mitosis) and S (synthesis), of various cell cycle phases help to understand the phase at which certain molecule is causing an arrest to exhibit its cytotoxic effect in comparison to control. HeLa cells treated with compound C1 at two concentrations 30 and 60 μM reduced the G_0/G_1 phase from 61.3% to 47.6 and 58.0% respectively while S phase is slightly increased from 14.4% to 19.8 and 17.2% respectively (Fig. 4) (**A1**-**C1**). When the same compound was treated against MCF-7 cell line reduction in G_0/G_1 phase was observed from 62.8% to 61.4 and 56.5% respectively while S phase increased from 14.4% to 19.8 and 17.2% respectively (Fig. 4) (**A1**-**C1**). A common mechanism for inducing G2/M cell cycle arrest was observed through DNA damage activation checkpoint which suggested that studied compounds may inhibit tumor growth by binding to DNA [60].

3.8. Interaction with biomolecules

DNA is a vital target for drug candidates especially for metal based drugs and therefore, drug-DNA interaction study could be a helpful tool to investigate mechanism or efficacy relatable with *In Vitro* screening of drugs [61]. Theoretical investigation of HOMO-LUMO gap also helps in predicting reactivity as well as mode of interaction with the target site. FMOs theory represents that HOMO -LUMO energy gap have a noteworthy effect on the biological potential of drug candidates [62]. Greater the energy gap greater will be the efficacy of the metal complex to interact with the target site, while the least HOMO energy gap led to the complex stability and results in lesser interaction to the biological site [63,64]. Investigated compounds have suitable energy levels which make them good electron donor due to the high HOMO energies, and results in showing good binding potential with studied targets. Overall results of binding interaction showed complex **C1** has more binding potential because of having high energy value that helps in strong binding potential with the target site due to easy charge transfer. Similar results were also reported in literature that higher the energy gap better the biological potential of studied compounds [5]. Molecular docking calculations for interaction of (**C1**-**C3**) with DNA predicts good binding potential which was experimentally studied through various spectroscopic techniques and viscosity based measurements [65]. Binding constant Kb was measured through UV–visible titrations monitoring at

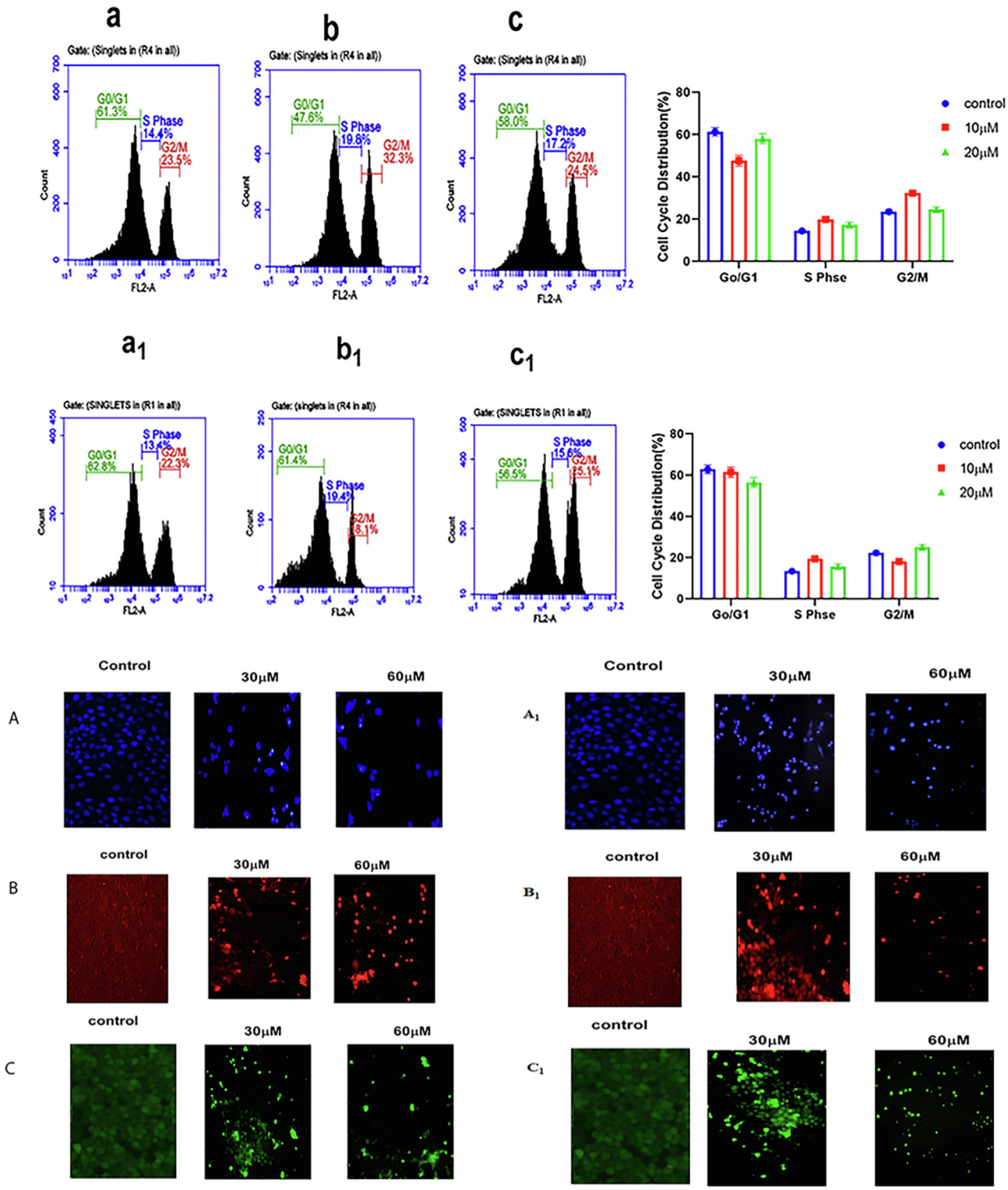

Fig. 4. Apoptosis induced by **C1** (A-C) on HeLa cells and (**A1**-**C1**) on MCF-7 cell line evaluated by cell cycle analysis using flow cytometry. Cytograms representing untreated and treated samples (10 μM, 20 μM) respectively, **A**,**A1**) Changes in nuclear morphology induced by 30 μM and 60 μM of **C1** for HeLa and MCF-7 respectively after treatment with DAPI compared to control untreated cells. **B**, **B1**) PI staining of apoptotic cells of Hela and MCF-7 strains respectively. **C**, **C1**) Oxidized DCF fluorescence in HeLa and MCF-7 cells induced by 30 μM and 60 μM of **C1** and untreated cells after treatment with 2′,7′- dichlorodihyd*rofluo*rescein diacetate.

260 nm and found 7.83×10^5 M^{-1} and 1.18×10^6 M^{-1} for **C1** and **C2** respectively and results are presented in (Fig. 5). Generally metal complexes can interact through multiple mechanisms, either through covalent or non-covalent bonding, adduct formation, modifications of phosphodiester linkages or cross linking with DNA etc. [66–68]. During the molecular spectroscopic titration, hypochromic and bathochromic shifts indicates intercalative binding while hyperchromic shift indicates tentative groove binding of drug with DNA. On gradual addition of increasing concentration of DNA in constant drug quantity, hypochromic shift was measured

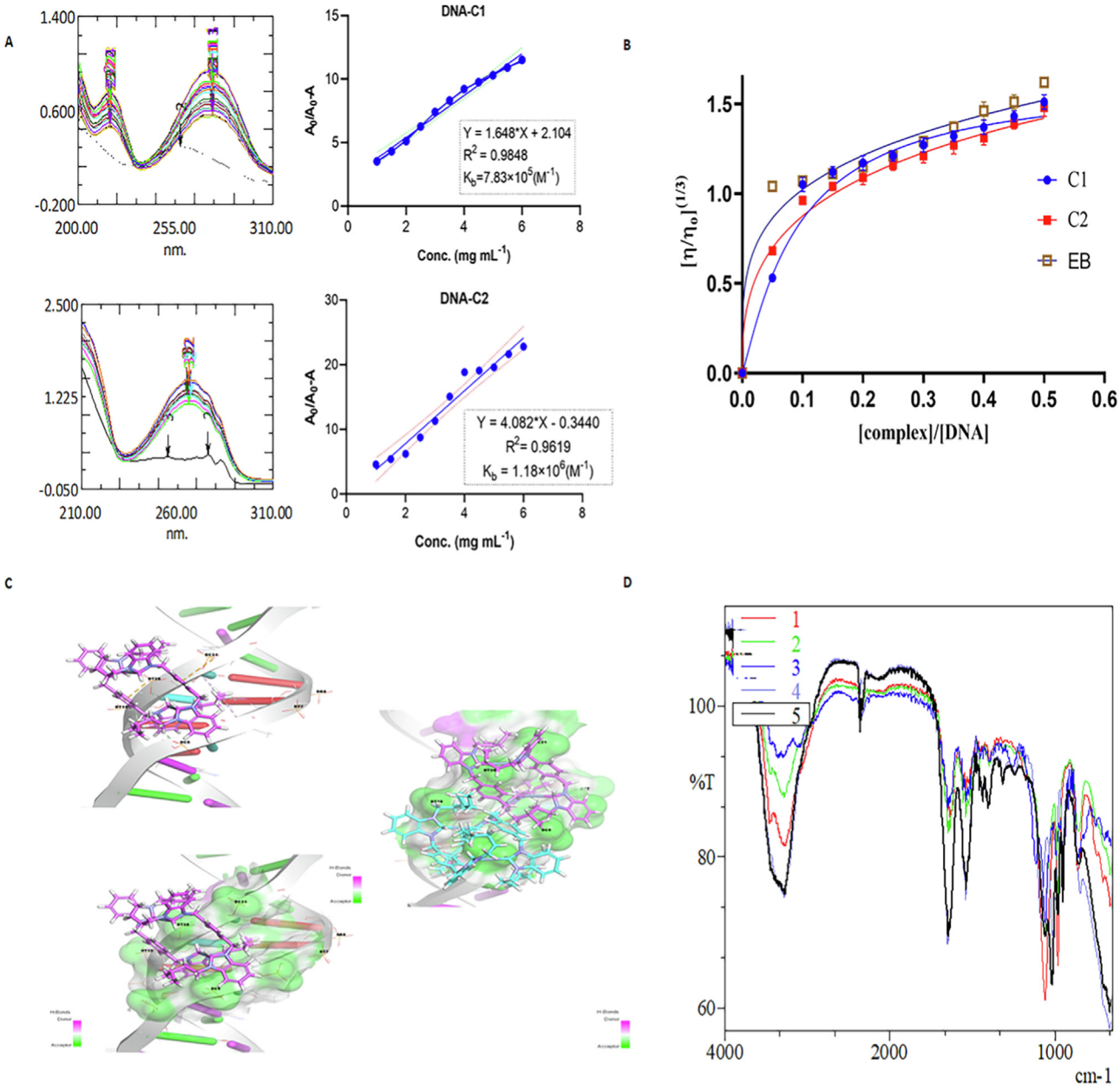

Fig. 5. **A**) UV–visible spectroscopic titrations for interaction of **C1** and **C2** with CT-DNA **B**) Relative viscosity experiment of complexes (**C1**-**C2**) and EB (ethidium Bromide) with ct-DNA, C) **3D** views of interactions of each complex (**C1**, pink, stick; **C2**, cyan, stick) against DNA and surface mapping of hydrogen bond donor/acceptor surface on DNA. D) FTIR spectroscopic titration of **C1** with ct-DNA. (For interpretation of the references to color in this figure legend, the reader is referred to the web version of this article.)

which indicates an intercalative mode of interaction of complexes with CT-DNA [69]. Spectroscopic studies showed shift in absorption pattern at 290 nm and 275 nm due to the Hydrogen bond breakage by the increase in DNA concentration while keeping drug concentration constant. Hyper-chromic shift in absorption was due to the intercalative mode of binding. The changes in absorption intensity for complex **(C1)** consist of two bands one occur at 220 nm intra ligand (IL) and the other metal–ligand transition (MLCT) at 290 nm (Fig. 5). The change in absorption intensity for complex **(C2)** due to the intra ligand (IL) took place at 210 nm and causes the hyperchromic effect of 260 nm while for metal to ligand transition (MLCT) change in absorption pattern was observed at 275 nm. This hypochromic shift could be due to changes in CT-DNA confirmation within the helix and may be contributed to the partial entrap of the aromatic ring into the helix. The possible red shift observed upon interaction with DNA could be relate with empty π^* orbital of the complex could overlap to the π-orbital of the CT-DNA base pairs [70]. Interaction of studied compounds with DNA was further probed through FTIR spectroscopy by observing shift in spectral pattern of DNA with addition of studied compounds. The most prominent bands observed in FTIR spectra of DNA at 1790–1580 cm^{-1} corresponds to nitrogenous bases and specifically sharp peak at 1650.1 cm^{-1} is assigned to carbonyl stretching of guanine. The slight shift and suppression in spectral band from 1650.1 cm^{-1} upon interaction of DNA and Ag (I)-complex **C1** could be attributed to interaction of **C1** with C=O of guanine or thymine moiety [71]. The other bands at 1529.1 cm^{-1} and 1545.7 cm^{-1} could be assigned to vibrational frequency of guanine and cytosine [26]. The specific bands appeared at 1024.3 cm^{-1} could be attributed to phosphate group and this frequency was merely shift upward 1048.7 cm^{-1} which indicates potential binding of **C1** with phosphate group could possibly through H-

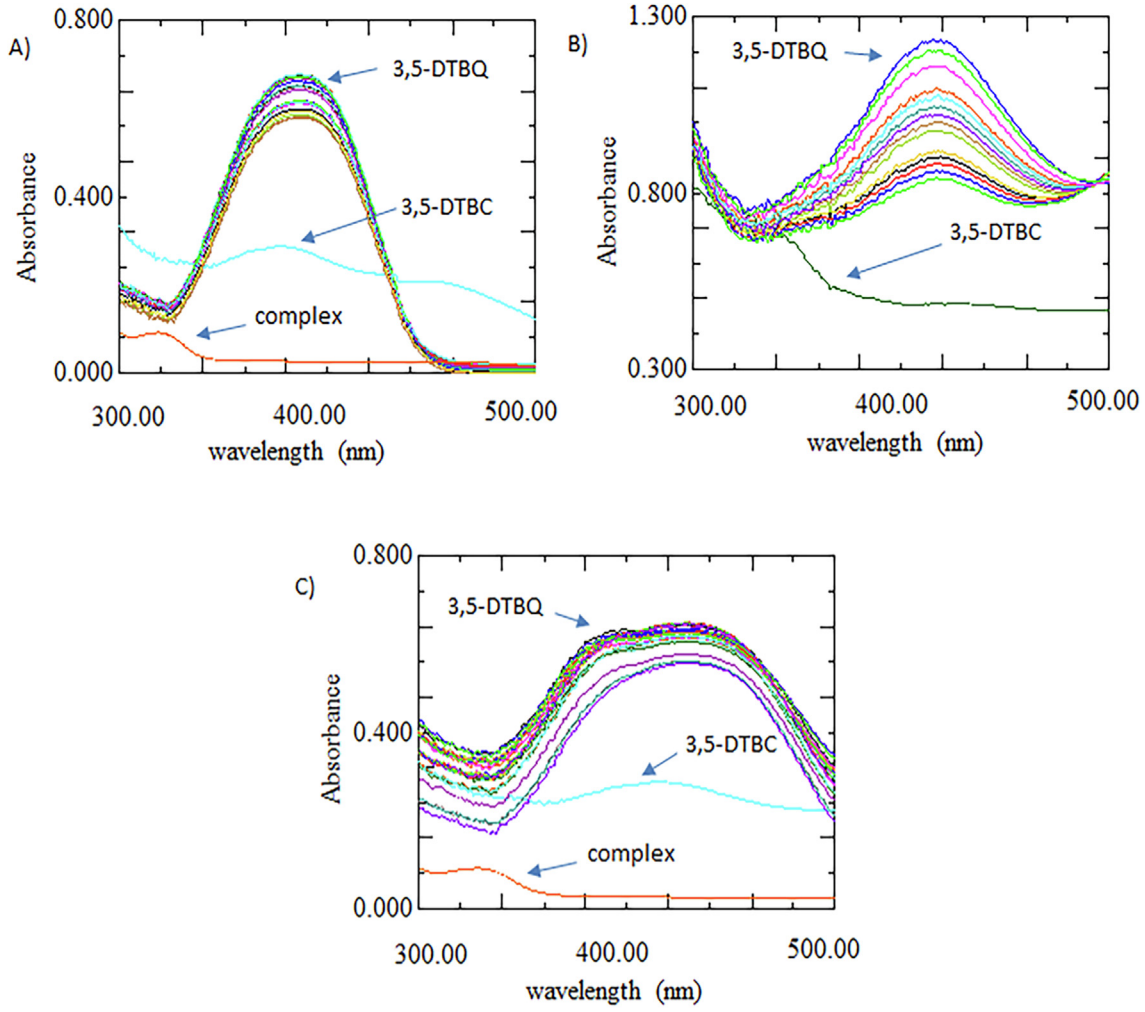

Fig. 6. UV–Visible spectra (300–500 nm) of reaction monitoring of complex C1 (1×10^{-4} M) and 100 folds of 3,5-DTBC (1×10^{-2} M) in different solvents A) Acetonitrile, B) Methanol and C) DMF.

bonding or electrostatic attraction. These observations confidently suggest that our studied compounds have tendency to potentially bind with DNA at their guanine base either via intercalative, through electrostatic or covalent bonding where labile ligand of complexes is exchanged with base pair of DNA [72]. These findings were also support our observations of UV spectral titration which claimed the potential binding of studied compounds with DNA through intercalative mode of binding.

Viscosity measurement of drug DNA mixture is an important tool to investigate the extent of binding of molecules. Although it could not predict exact mode of interaction but provides significant precision over mere changes in DNA which is helpful in combination with spectroscopic techniques to label the mode of interaction and binding strength. Change in viscosity of solution (DNA/drug) was measured with gradual addition of increasing amount of compounds separately and compared with positive control Ethidium bromide (EB), results are presented in Fig. 5**(B).** EB is well known standard for DNA intercalation which shows significant change in viscosity of solution upon mere addition of concentration via lengthening of DNA duplex. A similar and significant response was observed for our studied compounds which could indicate mimicry in binding mode of positive control. If the increase in viscosity made through DNA duplex lengthens which incorporate the exterior molecule for binding it infers intercalation mode of binding, while mere or no change could be assign as grooves or surface binding of drug with DNA [73,74]. Our results when compared with trend of literature indicates possible intercalative mode of binding which also supports the claim of spectroscopic studies. Among the studied compounds **C1** showed better response to viscosity measurements nearable to positive control. The trend of result was also observed in cytotoxicity of (**C1**-**C3)** which showed that biomolecular interactions could have possible impact on biological potential of designed compounds. Similar findings was also reported in our previous reports [8]. Studied compounds showed remarkably better results than standard drugs cisplatin having kb values 5.51×10^4 M^{-1} [75].

Serum albumin are supposed as carrier in blood stream plays a dominant role in drug distribution in the physiological stream [76]. Bovine serum albumin (BSA) mimics human serum albumin and therefore, can be used to probe interaction profile and could be a helpful tool in designing potent therapeutic agents [77]. Interaction of (**C1**-**C2)** with BSA was studied by spectrophotometer to monitor the shift in absorption pattern with the addition of complexes. The absorption spectra for these complexes are given in (**Fig. S37**)**.** Binding constant ($\mathbf{K_b}$) values of complexes (**C1**-**C2**) were investigated to evaluate their affinity for (BSA) and were found as $7.2 \times 10^6 M^{-1}$ and 4.44×10^6 M^{-1} respectively. The K_b value determined from the straight line equation indicates **C1** has more potential than **C2** to bind with BSA. Cytotoxicity of studied compounds was also observed in similar trend which indicates BSA interaction

Table 3
Kinetics parameters of catecholase activity in different solvents.

Complex	Solvent	V_{max}(10^{-4}M min^{-1})	K_M (10^{-4} M)	K_{cat} (h^{-1})
C1	Acetonitrile	0.197	0.0327	715.6
	Methanol	0.253	0.0636	904.8
	DMF	0.0265	0.0015	89.54
	DMSO	–	–	–

potential has some direct impact on biological activities of compounds. Our complexes showed better affinity for serum albumins than the reported Pd complexes in the literature which might be concerned to their coordination ability [78]. Studies showed that binding ability of the drugs very much depends upon the structural skelton that contributes towards its binding to the target site [79]. BSA interaction binding constants of test compounds were observed better than the reported similar mononuclear metal complex having Kb values upto 2×10^5 M^{-1} [9,79]. Interestingly our findings were even far better than the FDA approved chemotherapeutic agent like cisplatin Kb 8.52×10^2 M^{-1} [80].

3.9. Effect of solvent on catecholase activity

Catechol oxidase is an enzyme that catalyzes oxidation process of catechol to o-quinones coupled with reduction of oxygen to water molecule through a process known as catecholase activity. The In-vitro catalytic activity of metal complexes could be monitored through a reaction of test compounds with catechol. The product o-Quinone converted to melanin, a brownish pigment, through auto polymerization which can be monitored spectrophotometrically. Interestingly, catalytic activity of test compounds could possibly be affected by change in nature of medium solvent that could be understand through change in spectral response of reaction proceeding. In order to investigate the effect of solvent on catecholase activity, different organic solvents (methanol, acetonitrile, DMF and DMSO) were used. Catecholase activity of test compounds was performed on substrate 3,5-DTBC (3,5-di-*tert*-butylcatechol) to explore solvent dependent catalytic activity of test compounds. 3,5-DTBC bio-mimics oxidation reaction for metal complex due to low reduction potential, bulky structural nature and highly stable product of 3,5-di-*tert*-butylquinone (3,5-DTBQ). When this oxidation reaction of C1 with 3,5-DTBC studied in different solvents the resultant product 3,5-DTBQ showed different spectral response in terms of varied absorption wavelength at 401.6 nm, 403.8 nm and 399.8 nm for Methanol, acetonitrile and DMF respectively while DMSO did not respond for this reaction and results are given in Fig. 6**.** Spectrophotometric titrations of test compound (1×10^{-4} M) was made with 100 folds (1×10^{-4} M) of 3,5-DTBC separately in each solvent and reaction course was monitored for 2 h and spectral response is given in Fig. 6. The gradual increase in absorption with increasing reaction time was recorded at specific wavelength which indicates the rate of reaction for oxidation of catechol. The UV–Visible spectral behavior of reaction mixtures reveals that solvents has significant effect on catecholase activity of studied complexes. The solvent effect on catalytic activity could be linked with coordination ability of different solvents with reaction components. There is possible competition among solvent molecules and substrate to react with metal complex for catalytic activity. In this context, higher coordinating solvent results in less probable to substrate for reaction which reduced the catalytic activity of metal complexes for oxidation of catechol. Among the studied solvents, DMSO have higher coordinating ability therefore it adversely affects oxidation activity while methanol has least coordination and able to improve catalytic activity. The catalytic activity (Kcat) observed for compound C1 in different solvents is presented in Table 3. These results indicate that Methanol is better solvent to study catalytic activity while DMSO is not appreciable in this context. All these findings indicate the catecholase activity is solvent dependent and can be appreciably optimized through choice of suitable solvent. Our results were also supported by literature which reported that DMSO is not a choice for study of catecholase activity [81–83].

4. Conclusion

Here, six new compounds were synthesized, three azolium salts and three complexes, and characterized through UV–Visible, FTIR, ^{1}H&^{13}C NMR, FLR spectroscopy, elemental analysis and mass spectrometry. In order to understand the effect of solvent on catalytic activity of studied compounds, catecholase activity in three different solvents (methanol, acetonitrile, DMF and DMSO) was studied which suggested that Acetonitrile could be more suitable solvent for test compounds. Since, this class of compound has fascinating medicinal potential and this detailed report reveal the importance of lipophilic character and biomolecular interaction as possible factor to affect cytotoxicity of studied compounds. The solution phase stability of compounds (**C1**-**C3**) for a week through time dependent UV–Visible spectroscopy and HPLC-DAD and found stable for studied time period. The results of cytotoxicity of L1-L3 and (**C1**-**C3**) were screened by using MTT assay against HeLa, MCF-7, A549 and HCT-116 cancer cell lines and were further investigated through fluorescence microscopic assay as well as cell cycle assay by flow cytometry. A common mechanism for inducing G2/M cell cycle arrest was observed through DNA damage activation checkpoint which suggested that studied compounds may inhibit tumor growth by binding to DNA. The molecular docking calculations also anticipate the interaction of (**C1**-**C3**) with DNA and in comparison; **C1** was found more fastener having binding energy − 7.51 kcal/mol while **C2** of −4.3 kcal/mol. The experimental findings of spectroscopic titrations and viscosity measurements relates that **C1&C2** showed intercalative mode of binding with DNA with binding constant K_b of **C1** and C2,7.83 $\times$ $10^5$$M^{-1}$ and 1.18 $\times$ $10^6$$M^{-1}$ respectively. The BSA interaction of silver complexes was determined and moderate binding constant were observed. In this study, cytotoxicity and lipophilicity were correlated and precisely observed that ability to cross lipid layer affect directly the efficacy of cytotoxic compounds. Among the studied compounds, **C1** showed remarkably good anticancer activity IC_{50} 6.28 ± 0.82 μM in comparison to commonly used chemotherapeutic drugs cisplatin (8.74 ± 0.52 μM) against MCF-7 cell line. Altogether this study implies that silver complexes could be promising anticancer agents but it needs to screen through *In Vivo* studies and clinical trials.

CRediT authorship contribution statement

Rizwan Ashraf: Investigation, Data curation, Writing – original draft. **Ayesha Sarfraz:** Writing – review & editing. **Tugba Taskin-Tok:** Formal analysis, Resources. **Javid Iqbal:** Resources, Formal analysis. **Muhammad Adnan Iqbal:** Conceptualization, Methodology, Supervision. **Jamshed Iqbal:** Resources, Formal analysis. **Haq Nawaz Bhatti:** Supervision. **Mohamed El-Naggar:** Resources, For-

mal analysis. **Sumia Akram Revision:** . **Mohammad N. Murshed:** Resources. **Mohamed E. El Sayed:** Formal analysis. **Ahmed Samir:** .

Data availability

Data will be made available on request.

Declaration of Competing Interest

The authors declare that they have no known competing financial interests or personal relationships that could have appeared to influence the work reported in this paper.

Acknowledgment

The authors extend their appreciation to the Deanship of Scientific Research at King Khalid University for funding this work through General Research Project under grant number (RGP.1/193/43).

Appendix A. Supplementary data

Supplementary data to this article can be found online at https://doi.org/10.1016/j.molliq.2022.120921.

References

[1] B.A. Khakiani, F. Shirini, H. Tajik, H.T. Nahzomi, N. Daneshvar, J. Mol. Liq. 342 (2021).
[2] S. Gurusamy, K. Krishnaveni, M. Sankarganesh, R.N. Asha, A. Mathavan, J. Mol. Liq. 345 (2022).
[3] O.A. El-Gammal, A.A. El-Bindary, F.S. Mohamed, G.N. Rezk, M.A. El-Bindary, J. Mol. Liq. 346 (2022).
[4] M. Baron, S. Bellemin-Laponnaz, C. Tubaro, M. Basato, S. Bogialli, A. Dolmella, J. Inorg. Biochem. 141 (2014) 94.
[5] A. Sarfraz, R. Ashraf, S. Ali, T. Taskin-Tok, Z. Khalid, S. Ullah, T. Kahlid, M. Mushtaq, S.M. El-Bahy, Z.M. El-Bahy, J. Mol. Struct. 1251 (2022).
[6] K. Nomiya, S. Morozumi, Y. Yanagawa, M. Hasegawa, K. Kurose, K. Taguchi, R. Sakamoto, K. Mihara, N.C. Kasuga, Inorg. Chem. 57 (2018) 11322.
[7] B.Y. Lee, M.P. Sullivan, E. Yano, K.K. Tong, M. Hanif, T. Kawakubo-Yasukochi, S. M. Jamieson, T. Soehnel, D.C. Goldstone, C.G. Hartinger, Inorg. Chem. 60 (2021) 14636.
[8] R. Ashraf, H.N. Bhatti, M.A. Iqbal, Y. Jamil, Inorg. Chem. Commun. 119 (2020).
[9] R. Ashraf, Z. Khalid, A. Sarfraz, H.N. Bhatti, M.A. Iqbal, M. Nazari, J. Mol. Struct. 1241 (2021).
[10] R. Ashraf, M.A. Iqbal, H.N. Bhatti, M.R.S.A. Janjua, M. El-Naggar, ChemistrySelect 5 (2020) 10970.
[11] R. Ashraf, M. Javed, T. Taskin-Tok, R. Nadeem, M.K. Javaid, M. El-Naggar, O.M. Alzahrani, S.F. Mahmoud, Comput. Biol. Chem. 95 (2021).
[12] S.U. Parsekar, K. Paliwal, P. Haldar, P.S. Antharjanam, M. Kumar, Acs,, Omega (2022).
[13] Y. Zhang, A. Ho, J. Yue, L. Kong, Z. Zhou, X. Wu, F. Yang, H. Liang, Eur. J. Med. Chem. 86 (2014) 449.
[14] G. Sahu, A. Banerjee, R. Samanta, M. Mohanty, S. Lima, E.R. Tiekink, R. Dinda, Inorg. Chem. 60 (2021) 15291.
[15] R.A. Haque, M.A. Iqbal, F. Mohamad, M.R. Razali, J. Mol. Struct. 1155 (2018) 362.
[16] N. Marchand, P. Lienard, H.-U. Siehl, H. Izato, FUJITSU Sci Tech J 50 (2014) 46.
[17] V. Spassov, L. Yan, Proteins: Struct. Funct., Bioinformatics 81 (2013) 704.
[18] O. Trott, A.J. Olson, J. Comput. Chem. 31 (2010) 455.
[19] J. Eberhardt, D. Santos-Martins, A.F. Tillack, S. Forli, J. Chem. Inf. Model. 61 (2021) 3891.
[20] Y. Rose, J.M. Duarte, R. Lowe, J. Segura, C. Bi, C. Bhikadiya, L. Chen, A.S. Rose, S. Bittrich, S.K. Burley, J. Mol. Biol. 433 (2021).
[21] R. Sanchez, A. Šali, Curr. Opin. Struct. Biol. 7 (1997) 206.
[22] E.F. Pettersen, T.D. Goddard, C.C. Huang, G.S. Couch, D.M. Greenblatt, E.C. Meng, T.E. Ferrin, J. Comput. Chem. 25 (2004) 1605.
[23] G. Lv, L. Guo, L. Qiu, H. Yang, T. Wang, H. Liu, J. Lin, Dalton Trans. 44 (2015) 7324.
[24] M. Gaber, H.A. El-Ghamry, S.K. Fathalla, Appl. Organomet. Chem. 34 (2020) e5678.
[25] M. Feizi-Dehnayebi, E. Dehghanian, H. Mansouri-Torshizi, Spectrochim. Acta A Mol. Biomol. Spectrosc. 249 (2021).
[26] C. Baltazar, R. Mun, H. Tajmir-Riahi, J. Bariyanga, J. Mol. Struct. 1161 (2018) 273.
[27] D.M. Morgan, Polyamine protocols, Springer, 1998, pp. 179–184.
[28] A. Kamal, M. Nazari, M. Yaseen, M.A. Iqbal, M.B.K. Ahamed, A.S.A. Majid, H.N. Bhatti, Bioorg. Chem. 90 (2019).
[29] F.R. Noor Uddin, Saqib Ali,Syed Ahmed Tirmizi,Iqbal AhmadDepartment of Chemistry, Allama Iqbal Open University, Islamabad, Pakistan, J. Biomol. Struct. Dynam. (2019) 3246.
[30] N.U. Yoriko Saito, S. Tanaka, N. Suzuki, M. Tomizawa-Murasawa, A. Sone, Y. Najima, S. Takagi, Y. Aoki, A. Wake, S. Taniguchi, L.D. Shultz, F. Ishikawa, Nat. Biotechnol. (2010) pages275.
[31] J. Haribabu, S. Srividya, D. Mahendiran, D. Gayathri, V. Venkatramu, N. Bhuvanesh, R. Karvembu, Inorg. Chem. 59 (2020) 17109.
[32] H. Wu, Y. Zhang, C. Chen, J. Zhang, Y. Bai, F. Shi, X. Wang, New J. Chem. 38 (2014) 3688.
[33] P. Bera, A. Aher, P. Brandao, S.K. Manna, G. Mondal, A. Jana, A. Santra, H. Jana, P. Bera, Polyhedron 182 (2020).
[34] R.A. Haque, M.A. Iqbal, M.B.K. Ahamed, A.A. Majid, Z.A.A. Hameed, Chem. Cent. J. 6 (2012) 1.
[35] R. Gümüşada, M.E. Guenay, N. Özdemir, B. Cetinkaya, J. Coord. Chem. 69 (2016) 1463.
[36] M. Atif, H.N. Bhatti, R.A. Haque, M.A. Iqbal, M.B.A. Khadeer, A.M.S.A. Majid, Appl. Biochem. Biotechnol. 191 (2020) 1171.
[37] S. Şahin-Bölükbaşı, N. Şahin, M.N. Tahir, C. Arıcı, E. Çevik, N. Gürbüz, İ. Özdemir, B.S. Cummings, Inorg. Chim. Acta 486 (2019) 711.
[38] A. Sarfraz, R. Ashraf, S. Ali, T. Taskin-Tok, Z. Khalid, S. Ullah, T. Kahlid, M. Mushtaq, S.M. El-Bahy, Z.M. El-Bahy, J. Mol. Struct. (2021).
[39] M. Yaqoob, S. Gul, N.F. Zubair, J. Iqbal, M.A. Iqbal, J. Mol. Struct. 1204 (2020).
[40] M. Kaloğlu, N. Kaloğlu, İ. Özdemir, S. Günal, İ. Özdemir, Bioorg. Med. Chem. 24 (2016) 3649.
[41] S. Akkoç, I.Ö. Ilhan, Y. Gök, P.J. Upadhyay, V. Kayser, Inorg. Chim. Acta 449 (2016) 75.
[42] S. Roy, M. Böhme, S.P. Dash, M. Mohanty, A. Buchholz, W. Plass, S. Majumder, S. Kulanthaivel, I. Banerjee, H. Reuter, Inorg. Chem. 57 (2018) 5767.
[43] P. Adão, S. Majumder, S.P. Dash, S. Roy, M.L. Kuznetsov, J.C. Pessoa, C.S. Gomes, M.R. Hardikar, E.R. Tiekink, R. Dinda, Dalton Trans. 47 (2018) 11358.
[44] S.P. Dash, S. Pasayat, S. Bhakat, S. Roy, R. Dinda, E.R. Tiekink, S. Mukhopadhyay, S.K. Bhutia, M.R. Hardikar, B.N. Joshi, Inorg. Chem. 52 (2013) 14096.
[45] S. Roy, M. Mohanty, S. Pasayat, S. Majumder, K. Senthilguru, I. Banerjee, M. Reichelt, H. Reuter, E. Sinn, R. Dinda, J. Inorg. Biochem. 172 (2017) 110.
[46] P.G. Avaji, C.V. Kumar, S.A. Patil, K. Shivananda, C. Nagaraju, Eur. J. Med. Chem. 44 (2009) 3552.
[47] S. Roy, M. Mohanty, R.G. Miller, S.A. Patra, S. Lima, A. Banerjee, N. Metzler-Nolte, E. Sinn, W. Kaminsky, R. Dinda, Inorg. Chem. 59 (2020) 15526.
[48] S. Majumder, S. Pasayat, A.K. Panda, S.P. Dash, S. Roy, A. Biswas, M.E. Varma, B. N. Joshi, E. Garribba, C. Kausar, Inorg. Chem. 56 (2017) 11190.
[49] N. Naz, S. Saqib, R. Ashraf, M.I. Majeed, M.A. Iqbal, Maced. J. Chem. Chem. Eng. 39 (2020) 1.
[50] M. Atif, H.N. Bhatti, R.A. Haque, M.A. Iqbal, M.B. Ahamed Khadeer, A.M.S.A. Majid, Appl. Biochem. Biotechnol. 191 (2020) 1171.
[51] J.D. Aguirre, A.M. Angeles-Boza, A. Chouai, C. Turro, J.-P. Pellois, K.R. Dunbar, Dalton Trans. (2009) 10806.
[52] F. Arnesano, G. Natile, Coord. Chem. Rev. 253 (2009) 2070.
[53] L. Biancalana, L.K. Batchelor, T. Funaioli, S. Zacchini, M. Bortoluzzi, G. Pampaloni, P.J. Dyson, F. Marchetti, Inorg. Chem. 57 (2018) 6669.
[54] G. Agonigi, L. Biancalana, M.G. Lupo, M. Montopoli, N. Ferri, S. Zacchini, F. Binacchi, T. Biver, B. Campanella, G. Pampaloni, Organometallics 39 (2020) 645.
[55] S.H. van Rijt, A. Mukherjee, A.M. Pizarro, P.J. Sadler, J. Med. Chem. 53 (2010) 840.
[56] S.A. Patra, G. Sahu, P.D. Pattanayak, T. Sasamori, R. Dinda, Inorg. Chem. (2022).
[57] Y. Sun, Y. Li, S. Shi, C. Dong, Molecules 26 (2021) 2703.
[58] N. Uddin, F. Rashid, S. Ali, S.A. Tirmizi, I. Ahmad, S. Zaib, M. Zubair, P.L. Diaconescu, M.N. Tahir, J. Iqbal, J. Biomol. Struct. Dyn. 38 (2020) 3246.
[59] M. Shah, S. Nawaz, H. Jan, N. Uddin, A. Ali, S. Anjum, N. Giglioli-Guivarc'h, C. Hano, B.H. Abbasi, Mater. Sci. Eng. C 112 (2020).
[60] F. Rashid, N. Uddin, S. Ali, A. Haider, S.A. Tirmizi, P.L. Diaconescu, J. Iqbal, RSC Adv. 11 (2021) 4499.
[61] R. Hajian, N. Shams, M. Mohagheghian, J. Braz. Chem. Soc. 20 (2009) 1399.
[62] M. Hagar, H.A. Ahmed, G. Aljohani, O.A. Alhaddad, Int. J. Mol. Sci. 21 (2020) 3922.
[63] R.S. Borges, J.K. Vale, G.A. Pereira, A.A. Veiga, J.B. Junior, A.B. da Silva, Med. Chem. Res. 25 (2016) 852.
[64] R.S. Borges, T.G. Barros, G.A. Pereira, J. Batista Jr, R.F. Beleza Filho, A.A. Veiga, M. Hamoy, V.J. Mello, A.B. da Silva, C.A. Barros, Pharmacology & Pharmacy 5 (2014) 1185.
[65] R. Prabhakaran, P. Kalaivani, P. Poornima, F. Dallemer, G. Paramaguru, V.V. Padma, R. Renganathan, R. Huang, K. Natarajan, Dalton Trans. 41 (2012) 9323.
[66] Q.-L. Zhang, J.-G. Liu, H. Chao, G.-Q. Xue, L.-N. Ji, J. Inorg. Biochem. 83 (2001) 49.
[67] J. Błasiak, J. Kowalik, Acta Biochim. Pol. 48 (2001) 233.
[68] M. Mohanty, A. Banerjee, S. Biswal, A. Horn Jr, G. Schenk, K. Brzezinski, E. Sinn, H. Reuter, R. Dinda, J. Inorg. Biochem. 203 (2020).
[69] S.M. Leite, L.M. Lima, S. Gama, F. Mendes, M. Orio, I. Bento, A.n. Paulo, R. Delgado, O. Iranzo, Inorganic Chemistry 55 (2016) 11801.
[70] Q. Wei, J. Dong, P. Zhao, M. Li, F. Cheng, J. Kong, L. Li, J. Photochem. Photobiol. B Biol. 161 (2016) 355.
[71] M.K. Ahmed, F. Amiama, E.A. Sealy, Spectroscopy 23 (2009) 291.

[72] C. Banti, A. Giannoulis, N. Kourkoumelis, A. Owczarzak, M. Poyraz, M. Kubicki, K. Charalabopoulos, S. Hadjikakou, Metallomics 4 (2012) 545.
[73] S.K. Maiti, M. Kalita, A. Singh, J. Deka, P. Barman, Polyhedron 184 (2020).
[74] A.S. Alturiqi, E.S. Al-Farraj, M.M. Anazy, R.A. Ammar, J. Mol. Struct. 1219 (2020).
[75] C.N. N'soukpoé-Kossi, C. Descôteaux, É. Asselin, H.-A. Tajmir-Riahi, G. Bérubé, DNA Cell Biol. 27 (2008) 101.
[76] A. Roy, P. Seal, J. Sikdar, S. Banerjee, R. Haldar, J. Biomol. Struct. Dyn. 36 (2018) 387.
[77] R. Hosseinzadeh, K. Khorsandi, J. Biomol. Struct. Dyn. 34 (2016) 1903.
[78] P.S. Bangde, D.S. Prajapati, P.P. Dandekar, A.R. Kapdi, ChemistrySelect 3 (2018) 5709.
[79] J. Liu, Y. He, D. Liu, Y. He, Z. Tang, H. Lou, Y. Huo, X. Cao, RSC Adv. 8 (2018) 7280.
[80] C. Pérez-Arnaiz, J. Leal, N. Busto, M.C. Carrión, A.R. Rubio, I. Ortiz, G. Barone, B. Díaz de Greñu, J. Santolaya, J.M. Leal, Inorg. Chem. 57 (2018) 6124.
[81] I. Mantasha, M. Shahid, M. Kumar, A. Ansari, M.N. Akhtar, M.A. AlDamen, Y. Song, M. Ahmad, I.M. Khan, New J. Chem. 44 (2020) 1371.
[82] M.N. Ahamad, F. Sama, M.N. Akhtar, Y.-C. Chen, M.-L. Tong, M. Ahmad, M. Shahid, S. Hussain, K. Khan, New J. Chem. 41 (2017) 14057.
[83] M. Shahid, I. Mantasha, S. Khan, M. Mehtab, O. Yadav, A. Ansari, K.M. Qasem, A. Ahmed, M. Saniya, M.N. Akhtar, J. Mol. Struct. 1244 (2021).